PERGAMON

International Journal of Solids and Structures 38 (2001) 5117–5148

INTERNATIONAL JOURNAL OF SOLIDS and STRUCTURES

www.elsevier.com/locate/ijsolstr

Bifurcations of a coated, elastic cylinder

Davide Bigoni *, Massimiliano Gei

Dipartimento di Ingegneria Meccanica e Strutturale, Università di Trento, Via Mesiano 77, I-38050 Trento, Italy

Received 25 April 2000

Abstract

Bifurcations in velocities from a state of homogeneous axisymmetric deformation are investigated for a coated elastic cylinder subject to axial tension or compression. The cylinder and the finite-thickness coating have circular cross sections. At the coating/core contact, a linear interface is introduced to simulate imperfect bonding. The particular case in which the thickness of the coating becomes infinite is also addressed. This may model the behaviour of a fiber embedded in an infinite matrix. Generic modes of bifurcations are investigated in the elliptic range, comprised axi- and anti-symmetric modes. Incompressible, hyperelastic materials, including Ogden, Mooney–Rivlin, and J_2-deformation theory of plasticity, are considered in the applications.

Keywords: Axisymmetric deformation; Imperfect bonding; Bifurcations

1. Introduction

Foam-filled circular columns, thick sandwich-wall circular cylinders, coated bars and fibers are axisymmetric structures subject to tensile or compressive loads, which have been successfully employed in a broad range of applications, including naval, offshore and aeronautical construction and cable technologies. The load-carrying capacity of these structures is limited by the emergence of various failure patterns at different structural scale. These may include: global or local buckling, separation between layers, nucleation and growth of fractures. Accordingly, models at different levels of sophistication can be employed, ranging from structural mechanics-based approaches (Herrmann and Forrestal, 1965; Karam and Gibson, 1995; Budiansky, 1999) to numerical techniques (Hunt et al., 1999).

In this paper, an approach is developed which allows consideration of various bifurcation modes of different types. In particular, an axisymmetric geometry is considered, where a solid bar of circular cross section is connected through an imperfect interface to a coaxial, finite-thickness coating. Both the solid bar and the coating are composed of incompressible, transversely-isotropic materials sufficiently general to embrace, in addition to some hypoelastic solids not investigated, the hyperelastic cases of the Ogden material (and thus Mooney–Rivlin and neo-Hookean limits) and the J_2-deformation theory material. The

* Corresponding author. Tel.: +39-0461-882507; fax: +39-461-882599.
E-mail address: bigoni@ing.unitn.it (D. Bigoni).

0020-7683/01/$ - see front matter
PII: S0020-7683(00)00322-X

latter may model the behaviour of metals under proportional loading. The considered structure is subject to a homogeneous, axisymmetric, finite deformation inducing pure axial tension or compression. Before bifurcation, along the fundamental path, there is no interaction between the core and the coating, but interaction obviously occurs for bifurcation fields.

Bifurcations of the velocity problem are sought using the standard Trefftz criterion. This criterion has been successfully used in plane strain (Biot, 1965; Hill and Hutchinson, 1975; Young, 1976; Needleman, 1979; Triantafyllidis and Maker, 1985; Steif, 1986a,b, 1987; Needleman and Ortiz, 1991; Steigmann and Ogden, 1997) and axisymmetric problems (Wilkes, 1955; Fosdick and Shield, 1963; Cheng et al., 1971; Hutchinson and Miles, 1974; Bassani et al., 1980; Haughton and Ogden, 1979, 1980; Simpson and Spector, 1984; Miles and Nuwayhid, 1985; Davies, 1991; Chau, 1992, 1995; Pan and Beatty, 1997a,b; Chau and Choi, 1998). In the axisymmetric case, Wilkes (1955) and Pan and Beatty (1997a,b) analyze bifurcations of an incompressible, thick-walled tube subject to compression, Chau and Choi (1998) include a radial confining pressure (adopting constitutive equations useful for geomaterials), Haughton and Ogden (1979) extend the analysis to axial tension of a general class of rubber-like materials. Fosdick and Shield (1963) superimpose a small bending on finite axisymmetric deformation of a solid bar. Axisymmetric bifurcations of a circular cylinder are investigated by Cheng et al. (1971), Hutchinson and Miles (1974), Miles and Nuwayhid (1985) and Chau (1992). For an hyperelastic, compressible solid bar, subject to uniaxial compression, Simpson and Spector (1984) and Davies (1991) investigate the character of the equilibrium equations and give conditions for the existence of buckling or barrelling solutions of the bifurcation problem. Finally, Haughton and Ogden (1980) consider bifurcation of a cylinder rotating about its axis.

As far as the authors are aware, bifurcation of a coated, axially-loaded, cylindrical bar has been not yet considered. This is the goal of the present article. To allow the possibility of core/coating separation, an imperfect contact at the bar/coating interface is considered. The assumed contact model was proposed by Suo et al. (1992) and is simply a linear relation between the increment of nominal traction and the velocity jump across the interface. The same model was used by Bigoni et al. (1997) in a plane strain situation. Interestingly enough, the presence of the interface introduces one additional characteristic length in the problem.

The case when the elastic coating becomes infinitely thick is also explicitly analyzed. This may be important in the modelling of the behaviour of an isolated fiber in a composite.

In the problem analyzed in the present article, many particular situations may be obtained as limiting cases. For instance, when the core is vanishing stiff, bifurcations of the thick-walled tube analyzed by Wilkes (1955) and Pan and Beatty (1997a,b) are recovered. A similar situation occurs when the interfacial stiffness (between core and coating) is set equal to zero. In this case, the minimum bifurcation stretch is obtained between the core and the coating taken separately. Other interesting cases arise in the small and large wavelength limits, corresponding, respectively, to a kind of surface or interfacial wave-mode and to an Euler buckling-mode. In the former case, results are found which were given by Biot (1965) and Hutchinson and Tvergaard (1980).

As a general conclusion, we observe that the model presented in this article is able to capture a wide range of bifurcations enclosing: Euler buckling and barrelling for compression loads, necking-type bifurcations and high-frequency azimuthal modes for tensile loads, surface modes and shear banding both in tension and compression.

2. Field equations and constitutive relations

Quasi-static incremental deformation of a time-independent solid body is considered as a function of a time-like parameter controlling the deformation process. Equilibrium rate equations in the absence of body forces may be written as

$$\operatorname{Div}\dot{\mathbf{S}} = \mathbf{0}, \tag{1}$$

where the divergence operator is defined in the reference configuration for every second-order tensor field $\mathbf{A}$ and constant vector $\mathbf{a}$, such that $(\operatorname{Div}\mathbf{A})\cdot\mathbf{a} = \operatorname{Div}(\mathbf{A}^{\mathrm{T}}\mathbf{a})$ and $\dot{\mathbf{S}}$ is the material time derivative of the first Piola–Kirchhoff stress tensor $\mathbf{S}$, related to the Cauchy stress $\mathbf{T}$ through

$$\mathbf{S} = J\mathbf{T}\mathbf{F}^{-\mathrm{T}}, \tag{2}$$

where $\mathbf{F}$ is the deformation gradient and J its determinant. The material time derivative is

$$\dot{\mathbf{S}} = J\left(\dot{\mathbf{T}} + \mathbf{T}\operatorname{div}\mathbf{v} - \mathbf{T}\mathbf{L}^{\mathrm{T}}\right)\mathbf{F}^{-\mathrm{T}}, \tag{3}$$

where $\mathbf{v}$ is the spatial description of the velocity, $\mathbf{L}$, the velocity gradient and div denotes the spatial divergence operator.

An axisymmetric geometry with symmetry axis singled out by unit vector $\mathbf{e}_z$ will be analyzed. In particular, a cylindrical bar with an elastic coating will be considered. Across the coating/bar cylindrical contact surface, nominal traction must be continuous

$$[\![\dot{\mathbf{S}}]\!]\mathbf{e}_r = \mathbf{0}, \tag{4}$$

where the symbol $[\![\cdot]\!]$ denotes a jump of the relevant argument, i.e. $[\![\dot{\mathbf{S}}]\!] = \dot{\mathbf{S}}^{+} - \dot{\mathbf{S}}^{-}$ and $\mathbf{e}_r$ is the unit normal vector to the contact surface (thus $\mathbf{e}_r\cdot\mathbf{e}_z = 0$) directed toward the coating (denoted by $+$) and away from the core (denoted by $-$). In the case of a perfectly bonded interface, continuity of velocity $\mathbf{v}$

$$[\![\mathbf{v}]\!] = \mathbf{0} \tag{5}$$

must be imposed across the interface in addition to Eq. (4). However, we will use a more relaxed condition than Eq. (5), from which the latter can be obtained as a limit case. In particular, we adopt a simplified version of the model of linear interface proposed by Suo et al. (1992), in which the nominal traction rate at the interface is linearly related to the jump in velocity

$$\dot{\mathbf{S}}\mathbf{e}_r = k[\![\mathbf{v}]\!], \tag{6}$$

where $\dot{\mathbf{S}}\mathbf{e}_r$ stands for $\dot{\mathbf{S}}^{+}\mathbf{e}_r = \dot{\mathbf{S}}^{-}\mathbf{e}_r$ and k is a non-negative interfacial stiffness modulus, of dimension [stress/length]. In the original version of the Suo et al. model, employed also by Bigoni et al. (1997), k is replaced by a 3×3 stiffness matrix. A detailed explanation of model (6) is deferred to Appendix A.

Constitutive equations describe time-independent, incrementally linear mechanical behaviour of an *incompressible* and *transversely isotropic* material about axis $\mathbf{e}_z$ and may be expressed in terms of stress rate potential U as

$$\overset{\nabla}{\mathbf{T}} = \frac{\partial U(\mathbf{D},\mathbf{G},h_i)}{\partial\mathbf{D}} + \overset{\nabla}{p}\mathbf{I}, \quad \operatorname{tr}\mathbf{D} = 0 \tag{7}$$

where the symbol $(\overset{\nabla}{\ })$ denotes the Jaumann derivative of the relevant argument and $p = \operatorname{tr}\mathbf{T}/3$ is the mean Cauchy stress (playing the role of a Lagrange multiplier), so that $\overset{\nabla}{p} = \dot{p}$. The potential U depends on the Eulerian strain rate $\mathbf{D}$, on $\mathbf{G} = \mathbf{e}_z\otimes\mathbf{e}_z$, which condenses the directional, i.e. anisotropic, properties of the material (for stress-induced anisotropy, $\mathbf{e}_z$ coincides with the principal axis of Cauchy stress orthogonal to the isotropy plane) and on h_i, denoting a generic set of invariants representing the current state. Different choices of invariants h_i are possible, including principal stretches to describe stress induced elastic anisotropy and/or scalars to describe instantaneous strain hardening of deformation theory of plasticity.

Constitutive equations (7) describe a broad class of material behaviour including hyperelasticity and a subset of hypoelastic relations when $\mathbf{e}_z$ denotes a principal stress direction (Truesdell and Noll, 1965). Material frame indifference restricts the possible dependence of U on $\mathbf{D}$ and $\mathbf{G}$. In particular, it requires that the potential function U be an isotropic function of the two arguments $\mathbf{D}$ and $\mathbf{G}$, namely, that

$U(\mathbf{D},\mathbf{G}) = U(\mathbf{Q}\mathbf{D}\mathbf{Q}^{\mathrm{T}},\mathbf{Q}\mathbf{G}\mathbf{Q}^{\mathrm{T}})$, for every rotation $\mathbf{Q}$. This allows us to use the Spencer and Rivlin (1960) representation theorem for an isotropic scalar function of two symmetric, second-order tensors. Following Zysset and Curnier (1995) and retaining only the quadratic terms in $\mathbf{D}$ in the rate potential (7), one obtains

$$\overset{\nabla}{\mathbf{T}} = \mathbb{E}[\mathbf{D}] + \overset{\nabla}{p}\mathbf{I}, \tag{8}$$

where the fourth-order tensor $\mathbb{E}$ is the following function of $\mathbf{G}$

$$\mathbb{E} = \Gamma_1 \mathbf{I}\underline{\otimes}\mathbf{I} + \Gamma_2 \mathbf{G}\otimes\mathbf{G} + \Gamma_3(\mathbf{G}\underline{\otimes}\mathbf{I} + \mathbf{I}\underline{\otimes}\mathbf{G}) + \Gamma_4 \mathbf{I}\otimes\mathbf{G}, \quad \mathbf{G} = \mathbf{e}_z\otimes\mathbf{e}_z, \tag{9}$$

where symbol $\underline{\otimes}$ denotes, for every set of second-order tensors $\{\mathbf{A}, \mathbf{B}, \mathbf{C}\}$, the tensorial product

$$(\mathbf{A}\underline{\otimes}\mathbf{B})[\mathbf{C}] = \mathbf{A}\frac{\mathbf{C}+\mathbf{C}^{\mathrm{T}}}{2}\mathbf{B}^{\mathrm{T}}. \tag{10}$$

The following important remarks should be added to Eq. (9):

(1) Tensor $\mathbb{E}$ has both the minor symmetries.

(2) Tensor $\mathbb{E}$ has also the major symmetry. This becomes immediate by observing that, due to the incompressibility constraint $\mathrm{tr}\,\mathbf{D} = 0$, the term $\Gamma_4\,\mathbf{G}\otimes\mathbf{I}$ vanishes when applied to $\mathbf{D}$, and can therefore be added to the right-hand side of Eq. (9) without altering it.

(3) Incremental moduli Γ_j $(j = 1,\ldots,4)$ in Eq. (9) fully depend on the state through invariants h_i.

(4) Condition $\overset{\nabla}{p} = \mathrm{tr}\overset{\nabla}{\mathbf{T}}/3$ imposes the following relation between Γ_2, Γ_3, and Γ_4:

$$\Gamma_2 + 2\Gamma_3 + 3\Gamma_4 = 0, \tag{11}$$

so that Eq. (9) is defined by three independent Γ_j's only.

The incremental moduli Γ_j $(j = 1,\ldots,4)$ may be written equivalently as functions of another set of three independent incremental moduli, μ_1, μ_2 and μ_3 that will be used later

$$\Gamma_1 = 4\mu_2 - 2\mu_1, \qquad \Gamma_2 = 2\mu_1 + 2\mu_2 - 4\mu_3, \qquad \Gamma_3 = 2\mu_1 - 4\mu_2 + 2\mu_3, \qquad \Gamma_4 = 2\mu_2 - 2\mu_1. \tag{12}$$

The dependence of moduli Γ_j's (or, equivalently, μ_i's) on the current state can be obtained from different points of view. In particular, for an incompressible Cauchy elastic material, isotropic in its reference configuration, the Cauchy stress is an isotropic function of the left Cauchy–Green strain tensor $\mathbf{B} = \mathbf{F}\mathbf{F}^{\mathrm{T}}$

$$\mathbf{T} = -\pi\mathbf{I} + \alpha_1\mathbf{B} + \alpha_{-1}\mathbf{B}^{-1}, \tag{13}$$

where π represents an arbitrary hydrostatic pressure and α_1, α_{-1} are functions that depend on the principal stretches λ_1, λ_2 and λ_3, satisfying the incompressibility constraint $\lambda_1\lambda_2\lambda_3 = 1$.

Writing Eq. (13) with reference to the Eulerian principal axes yields α_1 and α_{-1}

$$\begin{aligned}
\alpha_1 &= \frac{1}{\lambda_1^2-\lambda_2^2}\left[\frac{(\sigma_1-\sigma_3)\lambda_1^2}{\lambda_1^2-\lambda_3^2} - \frac{(\sigma_2-\sigma_3)\lambda_2^2}{\lambda_2^2-\lambda_3^2}\right],\\
\alpha_{-1} &= \frac{1}{\lambda_1^2-\lambda_2^2}\left[\frac{\sigma_1-\sigma_3}{\lambda_1^2-\lambda_3^2} - \frac{\sigma_2-\sigma_3}{\lambda_2^2-\lambda_3^2}\right], \quad \lambda_1\lambda_2\lambda_3 = 1,
\end{aligned} \tag{14}$$

where $\sigma_i\,(i = 1,2,3)$ are the principal components of $\mathbf{T}$. The inequalities $\alpha_1 > 0$ and $\alpha_{-1} \leqslant 0$ are assumed to hold. If the material is hyperelastic, with strain energy function per unit reference volume $W(\lambda_1,\lambda_2,\lambda_3)$, the stress differences in Eq. (14) are given by

$$\sigma_1 - \sigma_3 = \lambda_1\frac{\partial\tilde{W}}{\partial\lambda_1}, \qquad \sigma_2 - \sigma_3 = \lambda_2\frac{\partial\tilde{W}}{\partial\lambda_2}, \tag{15}$$

where $\tilde{W}(\lambda_1,\lambda_2) = W(\lambda_1,\lambda_2,\lambda_1^{-1}\lambda_2^{-1})$.

The Ogden material (and thus the particular cases of Mooney–Rivlin and neo-Hookean materials), as well as the J_2-deformation theory of plasticity, correspond to different choices of strain energy function W. In particular:

(5) The incompressible Ogden material corresponds to the strain energy

$$W=\sum_{s=1}^{M}\frac{\beta_s}{\gamma_s}(\lambda_1^{\gamma_s}+\lambda_2^{\gamma_s}+\lambda_3^{\gamma_s}-3),\qquad 2\mu=\sum_{s=1}^{M}\beta_s\gamma_s,\quad \lambda_1\lambda_2\lambda_3=1, \tag{16}$$

where μ is the shear modulus in the ground state and β_s, γ_s are constitutive constant parameters ($\beta_s\gamma_s>0$, index not summed, Ogden, 1972). Mooney–Rivlin material corresponds to $M=2$, $\gamma_1=2$ and $\gamma_2=-2$ and neo-Hookean material to $M=1$, $\gamma_1=2$, so that $\beta_1=\mu$:

(6) The J_2-deformation theory material corresponds to the strain energy

$$W=\frac{K}{N+1}\varepsilon_e^{N+1},\qquad \varepsilon_e=\sqrt{\frac{2}{3}\left[(\ln\lambda_1)^2+(\ln\lambda_2)^2+(\ln\lambda_3)^2\right]},\quad \lambda_1\lambda_2\lambda_3=1\,, \tag{17}$$

where K is a constitutive stiffness parameter and N is an hardening exponent ($0<N\leqslant 1$).

In the axisymmetric geometry considered here, we identify λ_1 with λ_z and employ the symmetry $\lambda_2=\lambda_3=\lambda_z^{-1/2}$, so that the response functions α_1 and α_{-1} depend now only on the axial stretch λ_z. Taking the material time derivative of Eq. (13) and using the definition of Jaumann derivative, it is found that the incremental constitutive law can be expressed in the form (8) and (9) where (Appendix B)

$$\Gamma_1=2\left(\frac{\alpha_1}{\lambda_z}-\alpha_{-1}\lambda_z\right),\qquad \Gamma_2=\left(\lambda_z^2-\frac{1}{\lambda_z}\right)\left(\frac{\mathrm{d}\alpha_1}{\mathrm{d}\lambda_z}\lambda_z-\frac{\mathrm{d}\alpha_{-1}}{\mathrm{d}\lambda_z}\right),\qquad \Gamma_3=\left(\lambda_z^2-\frac{1}{\lambda_z}\right)\left(\alpha_1+\frac{\alpha_{-1}}{\lambda_z}\right), \tag{18}$$

and Γ_4 can be obtained from Eq. (11). In terms of the incremental moduli μ_i $(i=1,2,3)$ we have

$$\begin{aligned}
\mu_1&=\frac{1}{3}\left[\alpha_1\left(\frac{1}{\lambda_z}+2\lambda_z^2\right)-\alpha_{-1}\left(\frac{2}{\lambda_z^2}+\lambda_z\right)+\frac{\mathrm{d}\alpha_1}{\mathrm{d}\lambda_z}(\lambda_z^3-1)+\frac{\mathrm{d}\alpha_{-1}}{\mathrm{d}\lambda_z}\left(\frac{1}{\lambda_z}-\lambda_z^2\right)\right],\\
\mu_2&=\frac{1}{3}\left[\alpha_1\left(\frac{2}{\lambda_z}+\lambda_z^2\right)-\alpha_{-1}\left(\frac{1}{\lambda_z^2}+2\lambda_z\right)+\frac{1}{2}\frac{\mathrm{d}\alpha_1}{\mathrm{d}\lambda_z}(\lambda_z^3-1)+\frac{1}{2}\frac{\mathrm{d}\alpha_{-1}}{\mathrm{d}\lambda_z}\left(\frac{1}{\lambda_z}-\lambda_z^2\right)\right],\\
\mu_3&=\frac{1}{2}\left[\alpha_1\left(\frac{1}{\lambda_z}+\lambda_z^2\right)-\alpha_{-1}\left(\frac{1}{\lambda_z^2}+\lambda_z\right)\right].
\end{aligned} \tag{19}$$

The functions α_1, α_{-1} and the incremental moduli for the above material models are:

(7) Incompressible Ogden material:

$$\begin{aligned}
\alpha_1&=\frac{\lambda_z}{\lambda_z^3-1}\left[\frac{\lambda_z^3}{\lambda_z^3-1}\sum_{s=1}^{M}\beta_s\left(\lambda_z^{\gamma_s}-\lambda_z^{-\gamma_s/2}\right)-\frac{1}{2}\sum_{s=1}^{M}\beta_s\gamma_s\lambda_z^{-\gamma_s/2}\right],\ \alpha_{-1}\\
&=\frac{\lambda_z}{\lambda_z^3-1}\left[\frac{\lambda_z}{\lambda_z^3-1}\sum_{s=1}^{M}\beta_s\left(\lambda_z^{\gamma_s}-\lambda_z^{-\gamma_s/2}\right)-\frac{1}{2}\sum_{s=1}^{M}\beta_s\gamma_s\lambda_z^{1-\gamma_s/2}\right],\ \mu_1\\
&=\frac{1}{6}\sum_{s=1}^{M}\beta_s\gamma_s\left(2\lambda_z^{\gamma_s}+\lambda_z^{-\gamma_s/2}\right),\qquad \mu_2=\frac{1}{6}\sum_{s=1}^{M}\beta_s\gamma_s\left(\lambda_z^{\gamma_s}+2\lambda_z^{-\gamma_s/2}\right),\qquad \mu_3\\
&=\frac{1}{2}\frac{\lambda_z^3+1}{\lambda_z^3-1}\sum_{s=1}^{M}\beta_s\left(\lambda_z^{\gamma_s}-\lambda_z^{-\gamma_s/2}\right).
\end{aligned} \tag{20}$$

For the Mooney–Rivlin material equations (20) simplify to

$$\alpha_1 = \beta_1, \qquad \alpha_{-1} = \beta_2,$$
$$\mu_1 = \frac{1}{3}\left[\beta_1\left(\frac{1}{\lambda_z} + 2\lambda_z^2\right) - \beta_2\left(\frac{2}{\lambda_z^2} + \lambda_z\right)\right], \quad \mu_2 = \frac{1}{3}\left[\beta_1\left(\frac{2}{\lambda_z} + \lambda_z^2\right) - \beta_2\left(\frac{1}{\lambda_z^2} + 2\lambda_z\right)\right], \quad \mu_3 = \frac{\mu_1 + \mu_2}{2}, \tag{21}$$

so that for the neo-Hookean model (21) still hold with $\beta_2 = 0$;

(8) J_2-deformation theory solid:

$$\alpha_1 = K\varepsilon_e^{N-1}\frac{\lambda_z}{\lambda_z^3 - 1}\left(\frac{\lambda_z^3 \ln \lambda_z}{\lambda_z^3 - 1} - \frac{1}{3}\right), \qquad \alpha_{-1} = K\varepsilon_e^{N-1}\frac{\lambda_z^2}{\lambda_z^3 - 1}\left(\frac{\ln \lambda_z}{\lambda_z^3 - 1} - \frac{1}{3}\right),$$
$$\mu_1 = \frac{1}{3}KN\varepsilon_e^{N-1}, \qquad \mu_2 = \frac{1}{6}K(N+1)\varepsilon_e^{N-1}, \qquad \mu_3 = \frac{1}{2}K\varepsilon_e^{N-1}\frac{\lambda_z^3 + 1}{\lambda_z^3 - 1}\ln \lambda_z, \tag{22}$$

where $\varepsilon_e = |\ln \lambda_z|$. Note that the uniaxial stress–strain relation that may be obtained from Eq. (13) is simply $\sigma = K\varepsilon_e^{N-1} \ln \lambda_z$.

3. The problem

A circular cylinder with a coaxial circular coating is considered. In the initial, stress-free configuration the cylinder has radius R_c^- and height L and the coating has equal height, equal internal radius $R_c^+ = R_c^-$ and external radius R_e. Cylinder and coating are defined by the regions of the three-dimensional Euclidean space, respectively:

$$\begin{aligned} &0 \leqslant R \leqslant R_c^-, \qquad 0 \leqslant \Theta < 2\pi, \qquad 0 \leqslant Z \leqslant L, \\ &R_c^+ \leqslant R \leqslant R_e, \qquad 0 \leqslant \Theta < 2\pi, \qquad 0 \leqslant Z \leqslant L, \end{aligned} \tag{23}$$

where (R, Θ, Z) are cylindrical coordinates with the axis Z coincident with the axis of the cylinder. The condition $R_e \to \infty$ corresponds to the important situation of a cylinder embedded in an infinite matrix.

The structure is subjected to prescribed homogeneous axisymmetric deformation with principal stretch λ_z aligned with the axis of the cylinder. The current configuration is defined through cylindrical coordinates (r, θ, z), so that

$$r = \lambda_r R, \qquad \theta = \Theta, \qquad z = \lambda_z Z, \tag{24}$$

where λ_r, λ_θ and λ_z are the principal stretches, which, due to symmetry, satisfy $\lambda_\theta = \lambda_r$. The incompressibility constraint

$$\lambda_r \lambda_\theta \lambda_z = 1$$

allows us to express Eq. (24) as functions of the axial stretch only, namely

$$r = \lambda_z^{-1/2} R, \qquad \theta = \Theta, \qquad z = \lambda_z Z, \tag{25}$$

so that the current geometry is described by

$$r_c^- = r_c^+ = \lambda_z^{-1/2} R_c, \qquad r_e = \lambda_z^{-1/2} R_e, \qquad l = \lambda_z L. \tag{26}$$

Possibility of bifurcation from the deformed configuration (26) is investigated. A Lagrangean formulation of the field equations is adopted with the current configuration taken as reference, so that $\mathbf{F} = \mathbf{I}$ and $J = 1$.

The following boundary conditions are prescribed:

- null tractions at the external lateral surface of the coating

$$S_{rr} = \dot{S}_{rr} = 0, \quad S_{\theta r} = \dot{S}_{\theta r} = 0, \quad S_{zr} = \dot{S}_{zr} = 0, \qquad \text{at } r = r_e; \tag{27}$$

- imperfect contact at core/coating interface of the type (4) and (6)

$$[\![\dot{S}_{rr}]\!] = [\![\dot{S}_{\theta r}]\!] = [\![\dot{S}_{zr}]\!] = 0, \ \dot{S}_{rr} = k[\![v_r]\!], \qquad \dot{S}_{\theta r} = k[\![v_\theta]\!], \qquad \dot{S}_{zr} = k[\![v_z]\!], \qquad \text{at } r = r_c; \tag{28}$$

- perfectly smooth contact with a rigid, flat constraint on the faces $z = 0, l$

$$\dot{S}_{rz} = 0, \qquad \dot{S}_{\theta z} = 0, \qquad v_z = 0, \qquad \text{at } z = 0, l. \tag{29}$$

In the case when the elastic coating becomes infinitely thick, boundary conditions (27) at $r = r_e$ have to be replaced by the decay condition of the velocity

$$\mathbf{v} \to \mathbf{0} \quad \text{as} \quad r \to \infty. \tag{30}$$

Both the coating and the inner core are made up of the incompressible, transversely isotropic material defined by Eqs. (8) and (9). These equations become, in cylindrical coordinates

$$\begin{aligned}
&\dot{S}_{rr} = \dot{p} + 2\mu_2 L_{rr} + 2(\mu_1 - \mu_2)L_{\theta\theta}, && \dot{S}_{zz} = \dot{p} + 2(\mu_1 - \sigma)L_{zz},\\
&\dot{S}_{\theta\theta} = \dot{p} + 2\mu_2 L_{\theta\theta} + 2(\mu_1 - \mu_2)L_{rr}, && \dot{S}_{r\theta} = \dot{S}_{\theta r} = (2\mu_2 - \mu_1)(L_{r\theta} + L_{\theta r}),\\
&\dot{S}_{rz} = \left(\mu_3 + \frac{\sigma}{2}\right)L_{rz} + \left(\mu_3 - \frac{\sigma}{2}\right)L_{zr}, && \dot{S}_{zr} = \left(\mu_3 - \frac{\sigma}{2}\right)L_{rz} + \left(\mu_3 - \frac{\sigma}{2}\right)L_{zr},\\
&\dot{S}_{\theta z} = \left(\mu_3 + \frac{\sigma}{2}\right)L_{\theta z} + \left(\mu_3 - \frac{\sigma}{2}\right)L_{z\theta}, && \dot{S}_{z\theta} = \left(\mu_3 - \frac{\sigma}{2}\right)L_{\theta z} + \left(\mu_3 - \frac{\sigma}{2}\right)L_{z\theta},
\end{aligned} \tag{31}$$

where σ is the current Cauchy axial stress (that is different from core to coating) and the velocity gradient $\mathbf{L}$ has components

$$\begin{aligned}
&L_{rr} = v_{r,r}, && L_{r\theta} = \tfrac{1}{r}(v_{r,\theta} - v_\theta), && L_{rz} = v_{r,z},\\
&L_{\theta r} = v_{\theta,r}, && L_{\theta\theta} = \tfrac{1}{r}(v_r + v_{\theta,\theta}), && L_{\theta z} = v_{\theta,z},\\
&L_{zr} = v_{z,r}, && L_{z\theta} = \tfrac{v_{z,\theta}}{r}, && L_{zz} = v_{z,z},
\end{aligned} \tag{32}$$

where a comma denotes partial derivative. The incompressibility constraint becomes

$$\operatorname{tr}\mathbf{L} = v_{r,r} + \frac{1}{r}(v_r + v_{\theta,\theta}) + v_{z,z} = 0. \tag{33}$$

The above-described problem is governed by the scalar parameter λ_z, playing the role of time in the continuous, axisymmetric, quasi-static deformation defining the fundamental path. This path corresponds to uniaxial stress aligned with the axis of the cylinder and jumping across the interface. The boundary conditions (27)–(29) are trivially satisfied in the fundamental path, so as the equilibrium rate equations (1) which, in cylindrical coordinates, become

$$\begin{cases}
\dot{S}_{rr,r} + \frac{1}{r}\dot{S}_{r\theta,\theta} + \dot{S}_{rz,z} + \frac{\dot{S}_{rr} - \dot{S}_{\theta\theta}}{r} = 0,\\
\dot{S}_{\theta r,r} + \frac{1}{r}\dot{S}_{\theta\theta,\theta} + \dot{S}_{\theta z,z} + \frac{\dot{S}_{\theta r} + \dot{S}_{r\theta}}{r} = 0,\\
\dot{S}_{zr,r} + \frac{1}{r}\dot{S}_{z\theta,\theta} + \dot{S}_{zz,z} + \frac{\dot{S}_{zr}}{r} = 0.
\end{cases} \tag{34}$$

The introduction of two velocity potentials, $\Omega = \Omega(r, \theta, z)$ and $\Psi = \Psi(r, \theta, z)$, allows us to express the velocity components as

$$v_r = \Omega_{,rz} + \frac{\Psi_{,\theta}}{r}, \tag{35a}$$

$$v_\theta = \frac{\Omega_{,\theta z}}{r} - \Psi_{,r}, \tag{35b}$$

$$v_z = -\mathscr{M}(\Omega), \tag{35c}$$

where

$$\mathscr{M}(\cdot) = \frac{1}{r}(\cdot)_{,r} + (\cdot)_{,rr} + \frac{1}{r^2}(\cdot)_{,\theta\theta}$$

is the two-dimensional Laplacian operator in polar coordinates. It may be important to note that $v_\theta = 0$ and Ω and Ψ are independent of θ in the case of incremental axisymmetric deformations. In this special case, Eq. (35b) gives $\Psi = \Psi(z)$ and thus Ψ can be set equal to zero without loss of generality.

Through Eqs. (35a)–(35c) the incompressibility constraint is a priori satisfied. Substituting these into Eqs. (34) yields

$$\dot{p}_{,r} + C\mathscr{M}(\Omega)_{,rz} + D\left(\Omega_{,rzzz} + \frac{1}{r}\Psi_{,\theta zz}\right) + \frac{E}{r}\mathscr{M}(\Psi)_{,\theta} = 0, \tag{36a}$$

$$\dot{p}_{,\theta} + C\mathscr{M}(\Omega)_{,\theta z} + D(\Omega_{,\theta zzz} - r\Psi_{,rzz}) - Er\mathscr{M}(\Psi)_{,r} = 0, \tag{36b}$$

$$\dot{p}_{,z} - A\mathscr{M}^2(\Omega) - B\mathscr{M}(\Omega)_{,zz} = 0, \tag{36c}$$

where

$$A = \mu_3 - \frac{\sigma}{2}, \qquad B = 2\mu_1 - \mu_3 - \frac{\sigma}{2}, \qquad C = 2\mu_2 - \mu_3 + \frac{\sigma}{2}, \qquad D = \mu_3 + \frac{\sigma}{2}, \qquad E = 2\mu_2 - \mu_1.$$

Except in the case of incremental axisymmetric deformation (that will be considered later), the pressure rate $\dot{p}$ may be eliminated from Eqs. (36a)–(36c) deriving (36a) and (36b) with respect to θ and r, respectively, and subtracting the resulting equations. Analogously, (36b) and (36c) may be derived with respect to z and θ and subtracted. Assuming A, $E \neq 0$, we obtain

$$\begin{cases} \mathscr{M}\left[\left(\mathscr{M} + \rho_3^2 \frac{\partial^2}{\partial z^2}\right)\Psi\right] = 0, \\ \left[\left(\mathscr{M} - \rho_1^2 \frac{\partial^2}{\partial z^2}\right)\left(\mathscr{M} - \rho_2^2 \frac{\partial^2}{\partial z^2}\right)\Omega\right]_{,\theta} = r\frac{\rho_1^2\rho_2^2}{\rho_3^2}\left[\rho_3^2\Psi_{,zz} + \mathscr{M}(\Psi)\right]_{,rz}, \end{cases} \tag{37}$$

where coefficients ρ_1^2, ρ_2^2 (real or complex) depend, through the incremental moduli μ_1, μ_2, μ_3, on the axial stretch λ_z and are the solutions of the characteristic equation

$$A\rho^4 + (B + C)\rho^2 + D = 0. \tag{38}$$

The nature of roots $\pm\rho_1$ and $\pm\rho_2$ of Eq. (38) defines the regime classification:

- complex conjugate $\pm\rho_1$ and $\pm\rho_2$ in the elliptic complex (EC) regime;
- pure imaginary $\pm\rho_1$ and $\pm\rho_2$ in the elliptic imaginary (EI) regime;
- real $\pm\rho_1$ and $\pm\rho_2$ in the hyperbolic (H) regime;
- two real and two pure imaginary $\pm\rho_1$ and $\pm\rho_2$ in the parabolic (P) regime.

It should be noted that failure of ellipticity corresponds to the emergence of shear bands. Therefore, the investigation of bifurcation will be restricted in the present paper to the elliptic range, where $D > 0$, $E > 0$, so that the coefficient

$$\rho_3^2 = \frac{D}{E} = \rho_1^2\rho_2^2\frac{A}{E}$$

is always positive either in (EI) or in (EC) regimes. Moreover, $A > 0$.

In the special case of axisymmetric bifurcations, $\Psi = 0$, Eq. (36b) disappears, and (36a) and (36c) are independent of θ. Therefore, the pressure rate $\dot{p}$ may be eliminated from (36a) and (36c) deriving (36a) and (36c) with respect to z and r, respectively, and subtracting the resulting equations. Assuming $A \neq 0$, we obtain

$$\left[\left(\mathscr{M} - \rho_1^2\frac{\partial^2}{\partial z^2}\right)\left(\mathscr{M} - \rho_2^2\frac{\partial^2}{\partial z^2}\right)\Omega\right]_{,r} = 0, \tag{39}$$

where ρ_1^2 and ρ_2^2 are defined as in Eq. (37). Note that Hutchinson and Miles (1974) use Eq. (39) with a potential corresponding to our $-\Omega_{,r}$.

3.1. Bifurcation modes

Bifurcation in velocity is sought in the separate-variables form

$$\Omega(r,\theta,z) = \omega(r)\cos n\theta \sin \eta z, \tag{40a}$$

$$\Psi(r,\theta,z) = \psi(r)\sin n\theta \cos \eta z, \tag{40b}$$

$$\dot{p}(r,\theta,z) = q(r)\cos n\theta \cos \eta z, \tag{40c}$$

so that boundary conditions (29) are automatically satisfied. Obviously, the functions $\omega(r)$, $\psi(r)$ and $q(r)$ differ from cylinder to coating, but the longitudinal $\eta = \kappa\pi/l$ ($\kappa = 1, 2, \ldots$) and the circumferential n ($n = 0, 1, 2, \ldots$) wave numbers are assumed equal in the core and coating. These wave numbers fully define the bifurcation mode. Note that $n = 0$ corresponds to axisymmetric modes. An important aspect to be considered is that the choice Eqs. (40a)–(40c) rules out from the analysis all possible rigid body motions.

Substitution of Eqs. (40a) and (40b) into equilibrium equations (37) (note that Eq. (40c) giving $q(r)$ is for the moment not needed) gives

$$\begin{cases} \mathscr{L}_n^2(\psi) - \rho_3^2\eta^2\mathscr{L}_n(\psi) = 0, \\ (\mathscr{L}_n + \rho_1^2\eta^2)(\mathscr{L}_n + \rho_2^2\eta^2)\omega = \frac{r}{n}\eta\frac{\rho_1^2\rho_2^2}{\rho_3^2}\left(\mathscr{L}_n(\psi) - \rho_3^2\eta^2\psi\right)', \end{cases} \tag{41}$$

where a prime denotes differentiation with respect to r and

$$\mathscr{L}_n(\cdot) = (\cdot)'' + \frac{1}{r}(\cdot)' - \frac{n^2}{r^2}(\cdot)$$

is the Bessel operator. Introducing the function $\phi(r) = \mathscr{L}_n(\psi)$, Eq. (41a) becomes a modified Bessel equation of order n, namely

$$\mathscr{L}_n(\phi) - \rho_3^2\eta^2\phi = 0. \tag{42}$$

A solution of this can be written as

$$\phi(r) = \rho_3^2\eta^2[c_1 I_n(\rho_3\eta r) + c_2 K_n(\rho_3\eta r)], \tag{43}$$

where $I_n(x)$ and $K_n(x)$ are the modified Bessel functions of order n and c_1, c_2 are arbitrary constants.

Now, the solution to

$$\mathscr{L}_n(\psi) = \rho_3^2\eta^2[c_1 I_n(\rho_3\eta r) + c_2 K_n(\rho_3\eta r)] \tag{44}$$

is

$$\psi(r) = c_1 I_n(\rho_3\eta r) + c_2 K_n(\rho_3\eta r) + c_3 r^n + c_4 r^{-n}, \tag{45}$$

where c_i $(i = 1, \ldots, 4)$ are arbitrary constants.

Knowing $\psi(r)$, we may evaluate

$$(\mathscr{L}_n(\psi) - \rho_3^2\eta^2\psi)' = -c_3\rho_3^2\eta^2 n r^{n-1} + c_4\rho_3^2\eta^2 n r^{-n-1}, \tag{46}$$

which allows us to rewrite Eq. (41b) as

$$(\mathscr{L}_n + \rho_1^2\eta^2)(\mathscr{L}_n + \rho_2^2\eta^2)\omega = \eta^3\rho_1^2\rho_2^2(-c_3 r^n + c_4 r^{-n}). \tag{47}$$

The solution to Eq. (47) can be expressed equivalently in two ways,

$$\begin{cases} \omega(r) = -\frac{c_3}{\eta} r^n + \frac{c_4}{\eta} r^{-n} + a_1 J_n(\rho_1\eta r) + a_2 J_n(\rho_2\eta r) + a_3 Y_n(\rho_1\eta r) + a_4 Y_n(\rho_2\eta r), \\ \omega(r) = -\frac{c_3}{\eta} r^n + \frac{c_4}{\eta} r^{-n} + b_1 H_n^{(1)}(\rho_1\eta r) + b_2 H_n^{(1)}(\rho_2\eta r) + b_3 H_n^{(2)}(\rho_1\eta r) + b_4 H_n^{(2)}(\rho_2\eta r), \end{cases} \tag{48}$$

where $J_n(x)$ and $Y_n(x)$ are the Bessel and Neumann functions of order n, respectively, and $H_n^{(1)}(x)$ and $H_n^{(2)}(x)$ are the Hankel functions of order n. Moreover, the constants a_i and b_i $(i = 1, \ldots, 4)$ may be now complex and must be arranged in such a way that a real $\omega(r)$ always results for any value of ρ_1 and ρ_2. For instance, in the (EC) regime, where ρ_1 and ρ_2 are complex conjugate, the relations $J_n(\bar{x}) = \bar{J}_n(x)$, $Y_n(\bar{x}) = \bar{Y}_n(x)$ and $H_n^{(i)}(\bar{x}) = \bar{H}_n^{(j)}(x)$ $(i, j = 1, 2)$ imply $a_1 = \bar{a}_2$, $a_3 = \bar{a}_4$, $b_1 = \bar{b}_4$, and $b_2 = \bar{b}_3$, where a superposed bar denotes the complex conjugate.

It is important to note that a substitution in Eqs. (35a)–(35c) reveals that the terms r^n and r^{-n} in Eqs. (45) and (48) describe *a null velocity field*, so that they may be eliminated.

As a conclusion, the function $\psi(r)$ is

$$\psi(r) = c_1 I_n(\rho_3\eta r) + c_2 K_n(\rho_3\eta r), \tag{49}$$

while $\omega(r)$ takes one of the following form:

$$\omega(r) = a_1 J_n(\rho_1\eta r) + a_2 J_n(\rho_2\eta r) + a_3 Y_n(\rho_1\eta r) + a_4 Y_n(\rho_2\eta r), \tag{50a}$$

$$\omega(r) = b_1 H_n^{(1)}(\rho_1\eta r) + b_2 H_n^{(1)}(\rho_2\eta r) + b_3 H_n^{(2)}(\rho_1\eta r) + b_4 H_n^{(2)}(\rho_2\eta r). \tag{50b}$$

The expression (50a) will be used to describe $\omega(r)$ in the inner cylinder while Eq. (50b) will be used in the coating. This will facilitate the imposition of the boundary conditions.

In the special case of axisymmetric bifurcations $(n = 0)$, Eq. (39) yields

$$\left[(\mathscr{L}_0 + \rho_1^2\eta^2)(\mathscr{L}_0 + \rho_2^2\eta^2)\omega\right]' = 0, \tag{51}$$

which, except for an inconsequential constant, admits again the solution (50a) and (50b) with $n = 0$.

It may be observed that in all cases expressions (49) and (50a), (50b) are the solutions of

$$\begin{aligned} &(\mathscr{L}_n - \rho_3^2\eta^2)\psi = 0, \\ &(\mathscr{L}_n + \rho_1^2\eta^2)(\mathscr{L}_n + \rho_2^2\eta^2)\omega = 0. \end{aligned} \tag{52}$$

Representation (40a)–(40c) allows us to obtain $q(r)$, when used into Eq. (36c)

$$q(r) = B\eta\mathscr{L}_n(\omega) - \frac{A}{\eta}\mathscr{L}_n^2(\omega), \tag{53}$$

an expression still valid when $n = 0$.

A substitution of Eqs. (40a) and (40b) into Eqs. (35a)–(35c) yields the velocity field at bifurcation

$$v_r = f(r)\cos n\theta\cos\eta z, \qquad v_\theta = g(r)\sin n\theta\cos\eta z, \qquad v_z = h(r)\cos n\theta\sin\eta z, \tag{54}$$

where

$$f(r) = \eta\,\omega' + \frac{n}{r}\psi, \qquad g(r) = -\frac{\eta\, n}{r}\omega + \psi', \qquad h(r) = -\mathscr{L}_n(\omega). \tag{55}$$

Henceforth, superscripts $-$ and $+$ will denote quantities associated with the inner cylindrical core and with the external coating, respectively.

For the cylinder, the requirement of bounded solution along axis z (i.e. $r = 0$) provides the following simplification of Eqs. (50a), (50b) and (49)

$$\omega^-(r) = a_1^- J_n(\rho_1^-\eta r) + a_2^- J_n(\rho_2^-\eta r), \qquad \psi^-(r) = c_1^- I_n(\rho_3^-\eta r). \tag{56}$$

The expressions (49) and (50a), (50b) for $\psi(r)$ and $\omega(r)$ can be employed in Eqs. (55) and (53) to yield, for the cylinder

$$f^-(r) = a_1^-\left[\frac{\eta\, n}{r}J_n(\rho_1^-\eta r) - \rho_1^-\eta^2 J_{n+1}(\rho_1^-\eta r)\right] + a_2^-\left[\frac{\eta\, n}{r}J_n(\rho_2^-\eta r) - \rho_2^-\eta^2 J_{n+1}(\rho_2^-\eta r)\right] + c_1^-\frac{n}{r}I_n(\rho_3^-\eta r), \tag{57}$$

$$g^-(r) = -a_1^-\frac{\eta\, n}{r}J_n(\rho_1^-\eta r) - a_2^-\frac{\eta\, n}{r}J_n(\rho_2^-\eta r) - c_1^-\left[\frac{n}{r}I_n(\rho_3^-\eta r) + \rho_3^-\eta I_{n+1}(\rho_3^-\eta r)\right], \tag{58}$$

$$h^-(r) = a_1^-\rho_1^{-2}\eta^2 J_n(\rho_1^-\eta r) + a_2^-\rho_2^{-2}\eta^2 J_n(\rho_2^-\eta r), \tag{59}$$

$$q^-(r) = -a_1^-\rho_1^{-2}\eta^3(A^-\rho_1^{-2} + B^-)J_n(\rho_1^-\eta r) - a_2^-\rho_2^{-2}\eta^3(A^-\rho_2^{-2} + B^-)J_n(\rho_2^-\eta r), \tag{60}$$

and for the coating

$$\begin{aligned} f^+(r) = {} & b_1^+\left[\frac{\eta\, n}{r}H_n^{(1)}(\rho_1^+\eta r) - \rho_1^+\eta^2 H_{n+1}^{(1)}(\rho_1^+\eta r)\right] + b_2^+\left[\frac{\eta\, n}{r}H_n^{(1)}(\rho_2^+\eta r) - \rho_2^+\eta^2 H_{n+1}^{(1)}(\rho_2^+\eta r)\right] \\ & + b_3^+\left[\frac{\eta\, n}{r}H_n^{(2)}(\rho_1^+\eta r) - \rho_1^+\eta^2 H_{n+1}^{(2)}(\rho_1^+\eta r)\right] + b_4^+\left[\frac{\eta\, n}{r}H_n^{(2)}(\rho_2^+\eta r) - \rho_2^+\eta^2 H_{n+1}^{(2)}(\rho_2^+\eta r)\right] \\ & + c_1^+\frac{n}{r}I_n(\rho_3^+\eta r) + c_2^+\frac{n}{r}K_n(\rho_3^+\eta r), \end{aligned} \tag{61}$$

$$\begin{aligned} g^+(r) = {} & -b_1^+\frac{\eta\, n}{r}H_n^{(1)}(\rho_1^+\eta r) - b_2^+\frac{\eta\, n}{r}H_n^{(1)}(\rho_2^+\eta r) - b_3^+\frac{\eta\, n}{r}H_n^{(2)}(\rho_1^+\eta r) - b_4^+\frac{\eta\, n}{r}H_n^{(2)}(\rho_2^+\eta r) \\ & - c_1^+\left[\frac{n}{r}I_n(\rho_3^+\eta r) + \rho_3^+\eta I_{n+1}(\rho_3^+\eta r)\right] - c_2^+\left[\frac{n}{r}K_n(\rho_3^+\eta r) + \rho_3^+\eta K_{n+1}(\rho_3^+\eta r)\right], \end{aligned} \tag{62}$$

$$h^+(r) = b_1^+\rho_1^{+2}\eta^2 H_n^{(1)}(\rho_1^+\eta r) + b_2^+\rho_2^{+2}\eta^2 H_n^{(1)}(\rho_2^+\eta r) + b_3^+\rho_1^{+2}\eta^2 H_n^{(2)}(\rho_1^+\eta r) + b_4^+\rho_2^{+2}\eta^2 H_n^{(2)}(\rho_2^+\eta r), \tag{63}$$

$$\begin{aligned} q^+(r) = {} & -\rho_1^{+2}\eta^3(A^+\rho_1^{+2} + B^+)\left[b_1^+ H_n^{(1)}(\rho_1^+\eta r) + b_3^+ H_n^{(2)}(\rho_1^+\eta r)\right] - \rho_2^{+2}\eta^3(A^+\rho_2^{+2} + B^+) \\ & \times\left[b_2^+ H_n^{(1)}(\rho_2^+\eta r) + b_4^+ H_n^{(2)}(\rho_2^+\eta r)\right], \end{aligned} \tag{64}$$

where $a_i^{\mp}$, $b_j^{\mp}$ and $c_i^{\mp}$ $(i = 1,2;\ j = 1,\ldots,4)$ are arbitrary constants and the notation $\rho_i^{\mp 2}$ $(i = 1,2)$ stands for $(\rho_i^{\mp})^2$ $(i = 1,2)$.

Eqs. (57) and (64) fully specify the velocity field (54), which yields, through Eqs. (32) and (31), the material time derivative of the first Piola–Kirchhoff stress, namely

$$\begin{aligned}
\dot{S}_{rr} &= \left[q + 2\mu_2 f' + 2(\mu_1 - \mu_2)\left(\frac{f}{r} + n\frac{g}{r}\right)\right]\cos n\theta \cos \eta z,\\
\dot{S}_{\theta r} &= (2\mu_2 - \mu_1)\left(g' - n\frac{f}{r} - \frac{g}{r}\right)\sin n\theta \cos \eta z,\\
\dot{S}_{zr} &= \left(\mu_3 - \frac{\sigma}{2}\right)(h' - f\eta)\cos n\theta \sin \eta z.
\end{aligned} \tag{65}$$

3.2. The coated bar

The rate of nominal stress (65) depends, through functions $f^{\mp}(r)$, $g^{\mp}(r)$, $h^{\mp}(r)$, $q^{\mp}(r)$ on the nine unknown constants $a_i^{\mp}$, $b_j^{\mp}$ and $c_i^{\mp}$ $(i = 1, 2;\ j = 1, \ldots, 4)$. These may be now obtained imposing boundary conditions. For the coated cylinder, an homogeneous algebraic system is obtained in the form

$$[M^{\mathrm{C}}][a] = [0], \quad [a]^{\mathrm{T}} = [a_1^- \quad a_2^- \quad c_1^- \quad b_1^+ \quad b_2^+ \quad b_3^+ \quad b_4^+ \quad c_1^+ \quad c_2^+], \tag{66}$$

so that the bifurcation condition can be written as $\det[M^{\mathrm{C}}] = 0$ (matrix $[M^{\mathrm{C}}]$ is explicitly defined in Appendix C). Note that the determinant of $[M^{\mathrm{C}}]$ is always real or pure imaginary. Once the current geometry and state is known, the bifurcation mode has to be selected in terms of the circumferential wave number n, and of the three independent dimensionless parameters governing the formulation. These can be determined with elementary dimensional analysis considerations and reflect the characteristic lengths present in the problem, namely, the radius of the core, the thickness of the coating and the characteristic length related to the interface:

$$\eta r_{\mathrm{c}}, \qquad \frac{r_{\mathrm{e}}}{r_{\mathrm{c}}}, \qquad \hat{k} = \frac{k r_{\mathrm{c}}}{\mu_3^-}. \tag{67}$$

When the circumferential wave number, the relative stiffness of the materials and parameters (67) have been selected, the bifurcation condition can be numerically solved to give the critical values of axial stretch λ_z.

3.3. The fiber embedded in an infinite medium

It may be worth noting that in the specific case of infinite thickness of the coating, the decay condition of velocity implies that one coefficient of Eq. (49) and two of Eq. (50b) must be a priori null. In fact, for high values of the arguments x and y, we have

$$H_n^{(1)}(x) \sim \sqrt{\frac{2}{\pi x}}\mathrm{e}^{\mathrm{i}(x-(n+1)\pi/4)}, \tag{68a}$$

$$H_n^{(2)}(x) \sim \sqrt{\frac{2}{\pi x}}\mathrm{e}^{-\mathrm{i}(x-(n+1)\pi/4)}, \tag{68b}$$

$$I_n(y) \sim \sqrt{\frac{1}{2\pi y}}\mathrm{e}^{y}, \tag{68c}$$

$$K_n(y) \sim \sqrt{\frac{\pi}{2y}}\mathrm{e}^{-y}, \tag{68d}$$

where, in our case, $x = \rho_j^+ \eta r$ $(j = 1, 2)$ and $y = \rho_3^+ \eta r$. In the elliptic regime, since ρ_3^+ is a positive real number, (68c) shows that the first term of Eq. (49) becomes unbounded as $r \to \infty$ and hence c_1^+ must vanish. Moreover, the (EI) and (EC) regimes have to be considered separately for Eq. (50b). In the (EI) regime ρ_1^+ and ρ_2^+ are pure imaginary and $H_n^{(2)}(\rho_j^+ \eta r)$ $(j = 1, 2)$ becomes unbounded for large values of the

radius, so that coefficients b_3^+ and b_4^+ must vanish. In the regime (EC) ρ_1^+ and ρ_2^+ are complex conjugate, in the form $\delta + \mathrm{i}v$, $\delta - \mathrm{i}v$ respectively, with v positive real number. Thus the second and third term of (50b) become unbounded and b_2^+ and b_3^+ must be null. As a conclusion, in the elliptic regime the decay condition of velocity implies

$$c_1^+ = 0, \qquad \begin{cases} b_3^+ = b_4^+ = 0 & \text{(EI)}, \\ b_2^+ = b_3^+ = 0 & \text{(EC)}, \end{cases} \tag{69}$$

so that imposing boundary conditions yields the bifurcation criterion

$$\begin{cases} [M^{\mathrm{M,EI}}][a] = [0], \quad [a]^{\mathrm{T}} = [a_1^- \quad a_2^- \quad c_1^- \quad b_1^+ \quad b_2^+ \quad c_2^+] \quad \text{(EI)} \\ [M^{\mathrm{M,EC}}][a] = [0], \quad [a]^{\mathrm{T}} = [a_1^- \quad a_2^- \quad c_1^- \quad b_1^+ \quad b_4^+ \quad c_2^+] \quad \text{(EC)}, \end{cases} \tag{70}$$

where matrices $[M^{\mathrm{M,EI}}]$ and $[M^{\mathrm{M,EC}}]$ are specified in Appendix C.

4. Results

We report results obtained for Mooney–Rivlin material and J_2-deformation theory of plasticity. Tension and compression are analyzed in the latter case, whereas bifurcation in tension is excluded in the former case, which is therefore restricted to compression. In all cases we include the analysis of the limit corresponding to infinite thickness of the coating, simulating an isolated fiber in a continuum. It may be worth recalling that the analysis will be restricted to bifurcations occurring in the elliptic regime. Critical axial stretch λ_z at bifurcation is reported in Figs. 1–8, versus the product between the longitudinal wave number η and the radius of the inner core r_c, i.e. the dimensionless parameter ηr_c governing the bifurcation mode. Obviously, λ_z ranges between 1 and 0 in compression and is greater than 1 in tension. The critical circumferential mode n is indicated by a small number close to the relevant part of the curve and a spot denotes a transition between two different values of n. For material models of the type analyzed in this paper, the axial stretch is related to the axial Cauchy stress σ by

$$\frac{\sigma}{2\mu_3} = \frac{\lambda_z^3 - 1}{\lambda_z^3 + 1},$$

so that the axial stress at bifurcation may be easily evaluated from the critical stretch.

With the exception of Fig. 1, which is referred to the perfectly bonded case, different values of interfacial stiffness parameter $\hat{k}$ are considered, ranging between the extreme cases corresponding to perfectly bonded interface ($\hat{k} \to \infty$) and complete separation ($\hat{k} = 0$). Several well-known particular cases are recovered and discussed in detail below.

4.1. Mooney–Rivlin

For Mooney–Rivlin material loss of ellipticity with possible shear band formation, as well as bifurcations in tension are a priori excluded. Only uniaxial compression is therefore analyzed. The regime of the equilibrium equations is always (EI) with

$$\rho_1 = \mathrm{i}, \qquad \rho_2 = \mathrm{i}\lambda_z^{3/2}, \qquad \rho_3 = \lambda_z \sqrt{\frac{\lambda_z - \beta_2/\beta_1}{1 - \lambda_z^2 \beta_2/\beta_1}}.$$

The current axial stress (different from core to coating) is specified by

$$\sigma = \beta_1(\lambda_z^2 - \lambda_z^{-1}) + \beta_2(\lambda_z^{-2} - \lambda_z),$$

where β_1 and β_2 are related to the shear modulus μ through Eq. (16), namely, $\mu = \beta_1 - \beta_2$.

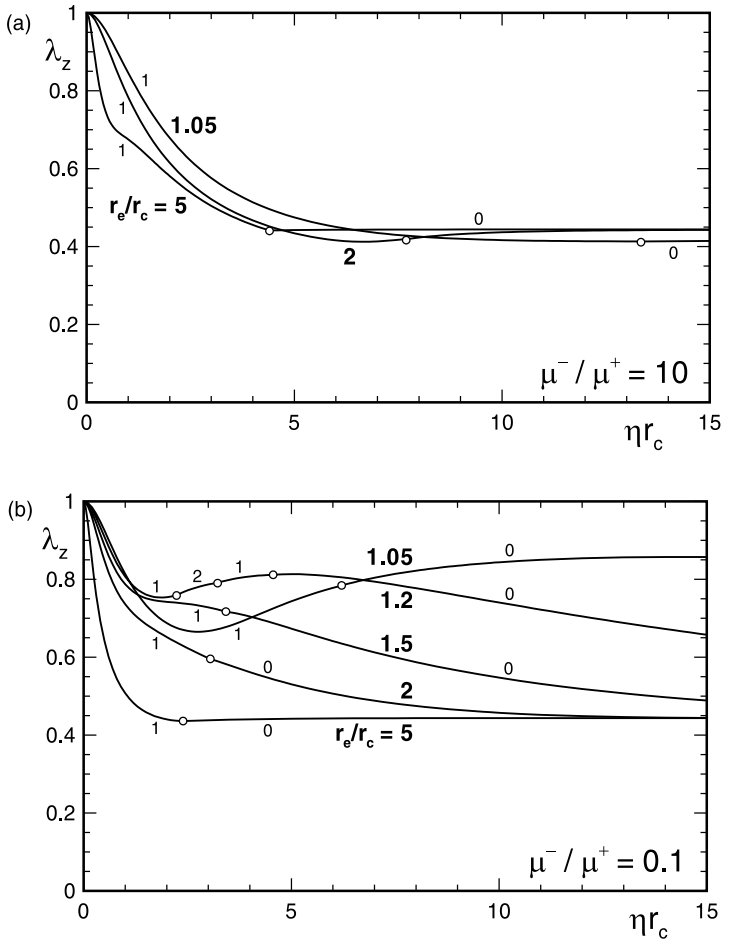

Fig. 1. Axial stretch at bifurcation (λ_z) for a coated elastic cylinder as a function of the core radius (r_c) multiplied by the bifurcation wave number (η). Various values of thickness of the coating (r_e/r_c) are considered. The coating and the core are both Mooney–Rivlin materials with $\beta_2/\beta_1 = -0.1$. A small number close to a curve denotes the critical circumferential mode, changing in correspondence of a spot on the curve. (a) The coating is weaker than the core, $\mu^-/\mu^+ = 10$. (b) The coating is stiffer than the core, $\mu^-/\mu^+ = 0.1$.

Figs. 1 and 2 are relative to the coated bar, whereas Fig. 3 refers to the elastic cylinder embedded in an infinite matrix. In all cases two incremental core/coating stiffness ratios μ^-/μ^+ are considered. In particular, parts (a) of the figures pertain to a more compliant coating on a stiffer core ($\mu^-/\mu^+ = 10$). Vice versa, parts (b) of the figures pertain to a stiffer coating on a more compliant core ($\mu^-/\mu^+ = 0.1$). Moreover, the investigation is limited to $\beta_2/\beta_1 = -0.1$.

Fig. 1 refers to a perfectly bonded interface and different values of coating thickness are investigated, ranging from $r_e/r_c = 1.05$ to $r_e/r_c = 5$. Three curves are reported in Fig. 1(a) lying in a narrow band. These exhibit the same features, namely, for small values of ηr_c the dominant mode is antisymmetric ($n = 1$), whereas the symmetric mode ($n = 0$) prevails for high longitudinal frequencies. The transition point between $n = 1$ and $n = 0$ varies from $\eta r_c \approx 4.40$, for $r_e/r_c = 5$, to $\eta r_c \approx 13.34$, for $r_e/r_c = 1.05$. All curves approach Euler buckling as $\eta r_c \to 0$ and the surface instability as $\eta r_c \to \infty$, the latter corresponding to $\lambda_z \approx 0.444$. It may be important to note that in the small wavelength limit two situations can occur, cor-

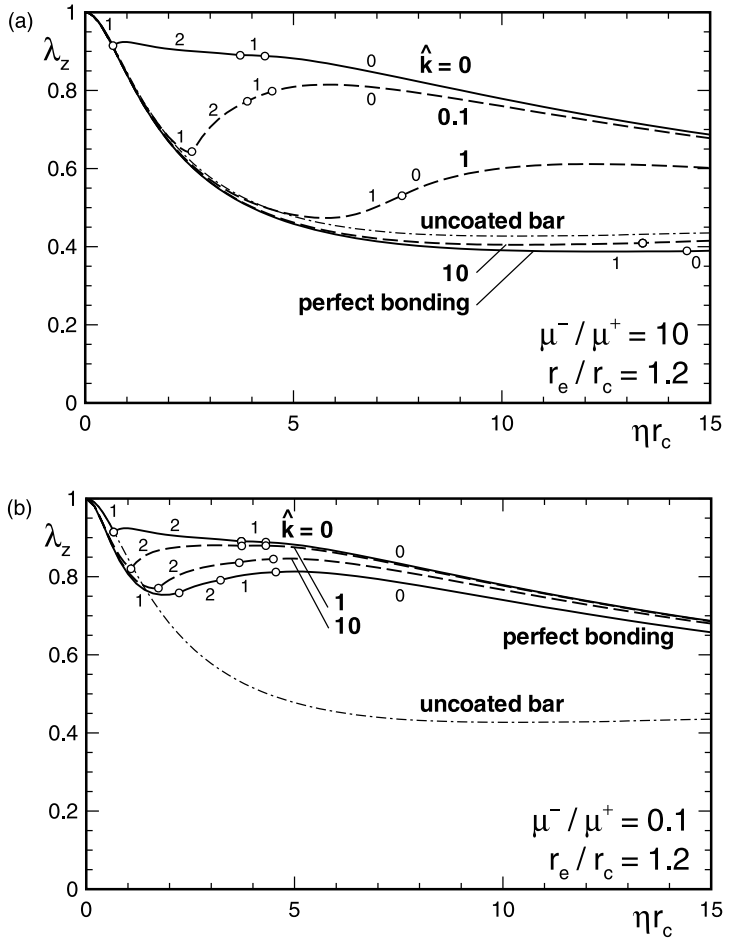

Fig. 2. Axial stretch at bifurcation (λ_z) for a coated elastic cylinder ($r_e/r_c = 1.2$) as a function of the core radius (r_c) multiplied by the bifurcation wave number (η). Various values of interfacial stiffness $\hat{k}$ are considered. The coating and the core are both Mooney–Rivlin materials with $\beta_2/\beta_1 = -0.1$. A small number close to a curve denotes the critical circumferential mode, changing in correspondence of a spot on the curve. (a) The coating is weaker than the core, $\mu^-/\mu^+ = 10$. (b) The coating is stiffer than the core, $\mu^-/\mu^+ = 0.1$.

responding either to the surface instability of the coating or to the interfacial instability at core/coating interface. For Mooney–Rivlin material, these two situations have been analyzed in detail by Biot (1965) and have been shown to differ from those pertaining to plane strain. In particular, for cylindrical geometry, surface and interfacial instabilities correspond to a plane strain incremental deformation superimposed on a current situation where the material is free to expand in the transverse direction. For the stiffness ratios considered in Figs. 1–3, i.e. $\mu^-/\mu^+ = 10$ and $\mu^-/\mu^+ = 0.1$, the interfacial instability occurs at $\lambda_z \approx 0.392$, so that the critical condition for high-frequency bifurcation is the surface instability limit, $\lambda_z \approx 0.444$. Compared to Fig. 1(a), the effect of the thickness of the coating is more evident in Fig. 1(b) ($\mu^-/\mu^+ = 0.1$), even if the long and short longitudinal wavelength limits remain the same. The curve relative to $r_e/r_c = 1.2$ in Fig. 1(b) differs from the others because there is a small range of values of ηr_c (between 2.23 and 3.22) where the critical circumferential mode corresponds to $n = 2$. A detailed analysis (not reported here) has revealed that a similar feature is shared by all curves with r_e/r_c ranging between 1.08 and 1.27. It may be observed

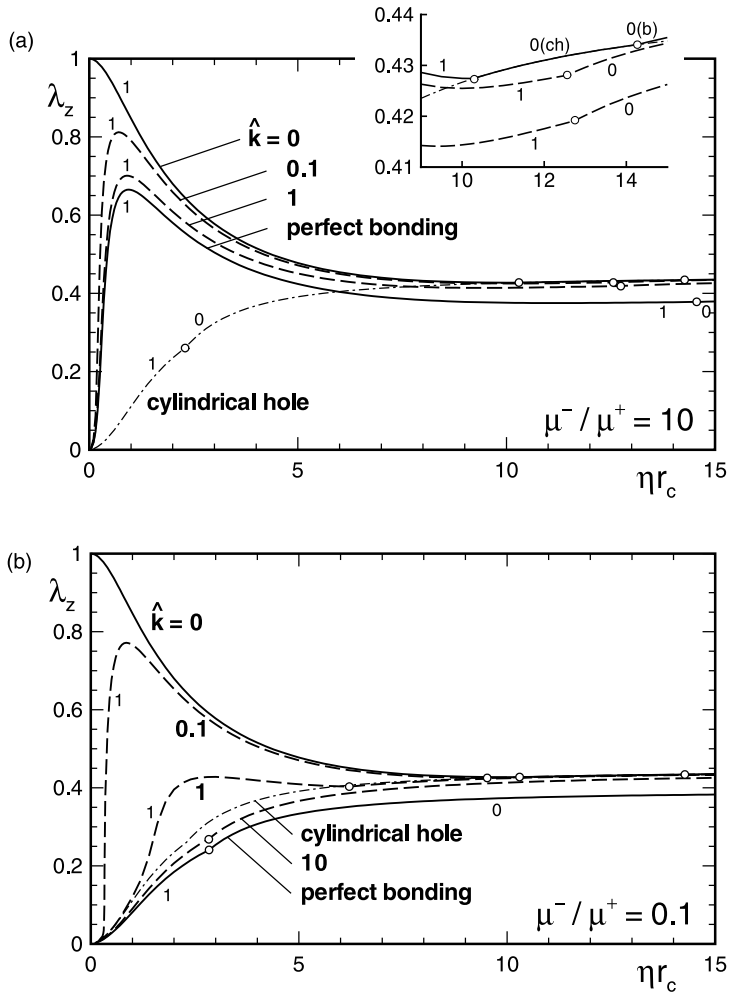

Fig. 3. Axial stretch at bifurcation (λ_z) for an elastic cylinder embedded in an infinite elastic matrix as a function of the core radius (r_c) multiplied by the bifurcation wave number (η). Various values of interfacial stiffness $\hat{k}$ are considered. The coating and the core are both Mooney–Rivlin materials with $\beta_2/\beta_1 = -0.1$. A small number close to a curve denotes the critical circumferential mode, changing in correspondence of a spot on the curve. (a) The coating is weaker than the core, $\mu^-/\mu^+ = 10$. In the separate detail the transition between antisymmetric and axisymmetric modes is evidenced for $\hat{k} = 0$, 0.1, 1. '0(ch)' and '0(b)' stand for axisymmetric mode relative to a cylindrical hole and to a bar, respectively. (b) The coating is stiffer than the core, $\mu^-/\mu^+ = 0.1$.

from Fig. 1(b) that, with the exception of the curve relative to $r_e/r_c = 1.05$, the thicker is the coating, the lower is the bifurcation stretch, for the reported range of ηr_c.

An interesting particular in the graph is that the minimum bifurcation stretch relative to the thin coating ($r_e/r_c = 1.05$) is smaller than that relative to a thicker coating ($r_e/r_c = 1.2$), at the value $\eta r_c = 2.78$. More in the detail, if we define the total axial load P_{tot} of the coated cylinder as

$$\frac{P_{tot}}{\pi r_c^2} = \sigma^- + \sigma^+ \left(\frac{r_e^2}{r_c^2} - 1 \right),$$

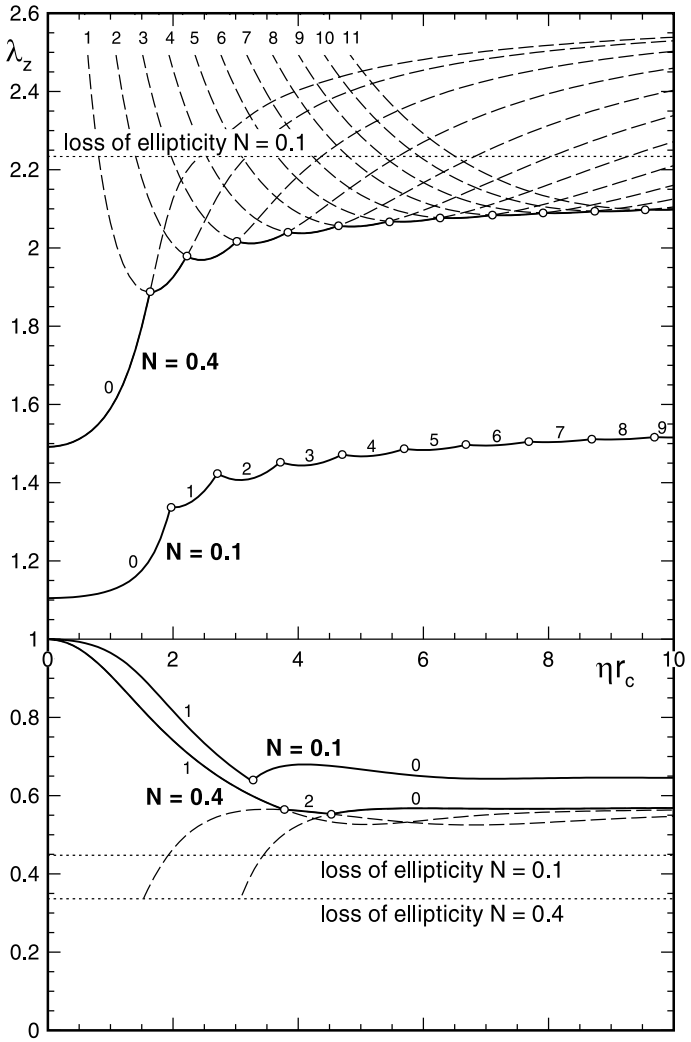

Fig. 4. Axial stretch at bifurcation (λ_z) for an elastic cylinder as a function of the core radius (r_c) multiplied by the bifurcation wave number (η). A small number close to a curve denotes the critical circumferential mode, changing in correspondence of a spot on the curve. J_2-deformation theory material is considered for $N = 0.1$ and 0.4.

we may conclude that the total axial load relative to $r_e/r_c = 1.2$ is 1.66 times greater than that relative to $r_e/r_c = 1.05$.

Fig. 2 is relative to a coated bar ($r_e/r_c = 1.2$) with a compliant interface between core and coating. Different values of the interfacial stiffness parameter $\hat{k}$ are considered, ranging between the extreme case of separation ($\hat{k} = 0$) and perfect bonding ($\hat{k} \to \infty$). The core is stiffer than the coating in Fig. 2(a), where the effects of the interfacial compliance are qualitatively and quantitatively important. The curve referred to the inner bar without coating is also reported in the figure for comparison (labelled as 'uncoated bar'). The antisymmetric ($n = 1$) and the axisymmetric ($n = 0$) critical circumferential modes are the only relevant bifurcation modes in the perfectly bonded case and for $\hat{k} = 10$ and $\hat{k} = 1$. The situation is more complicated for $\hat{k} = 0.1$ and $\hat{k} = 0$. In the former case there is a small range of values of ηr_c (between 2.56 and 3.89)

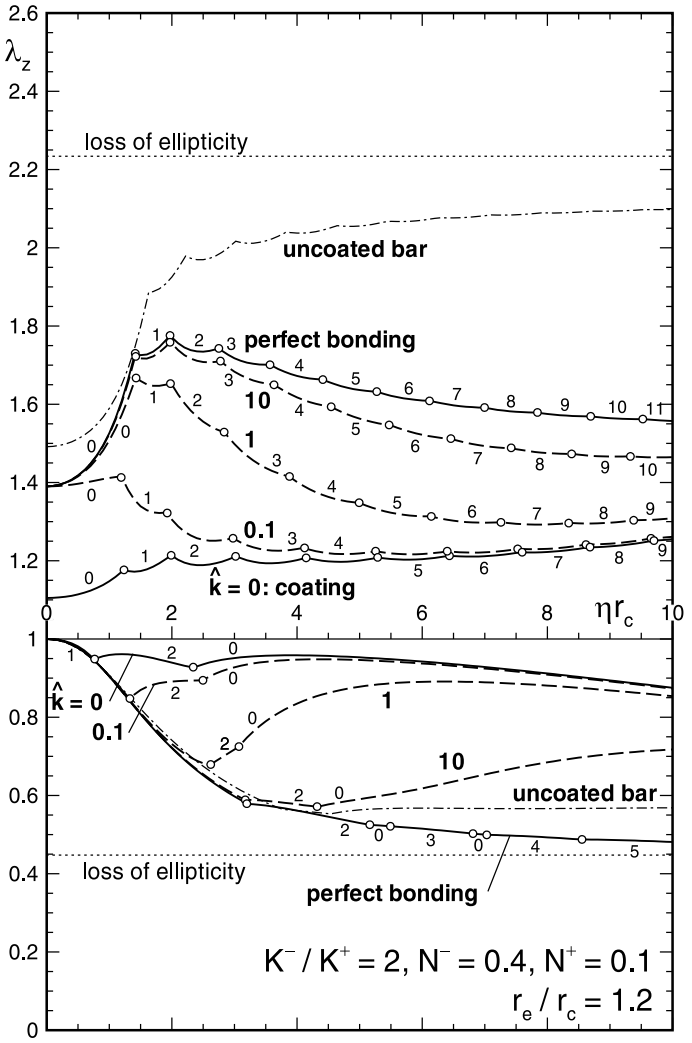

Fig. 5. Axial stretch at bifurcation (λ_z) for a coated elastic cylinder ($r_e/r_c = 1.2$) as a function of the core radius (r_c) multiplied by the bifurcation wave number (η). Various values of interfacial stiffness $\hat{k}$ are considered. A small number close to a curve denotes the critical circumferential mode, changing in correspondence of a spot on the curve. The coating and the core are both J_2-deformation theory materials with $K^-/K^+ = 2$, $N^- = 0.4$ and $N^+ = 0.1$.

where the mode $n = 2$ becomes critical. The latter case, $\hat{k} = 0$, corresponding to complete separation, is the combination of the bifurcation stretches relative to the inner bar and the external coating taken separately. In particular, for $0 < \eta r_c \leqslant 0.67$ the critical condition is attained by the solid bar (with antisymmetric mode), whereas for $\eta r_c > 0.67$ bifurcations are due to the isolated coating. Previous investigations of bifurcation of a hyperelastic tube subject to axial loading were restricted to axisymmetric and antisymmetric modes (Wilkes, 1955; Pan and Beatty, 1997a,b). We find here that the mode $n = 2$ becomes critical in a significant range of ηr_c, for $r_e/r_c = 1.2$. For a Mooney–Rivlin material with $\beta_2/\beta_1 = -0.1$ this always happens for ratios $r_e/r_c < 1.55$. Moreover, for decreasing values of the ratio r_e/r_c, higher-order

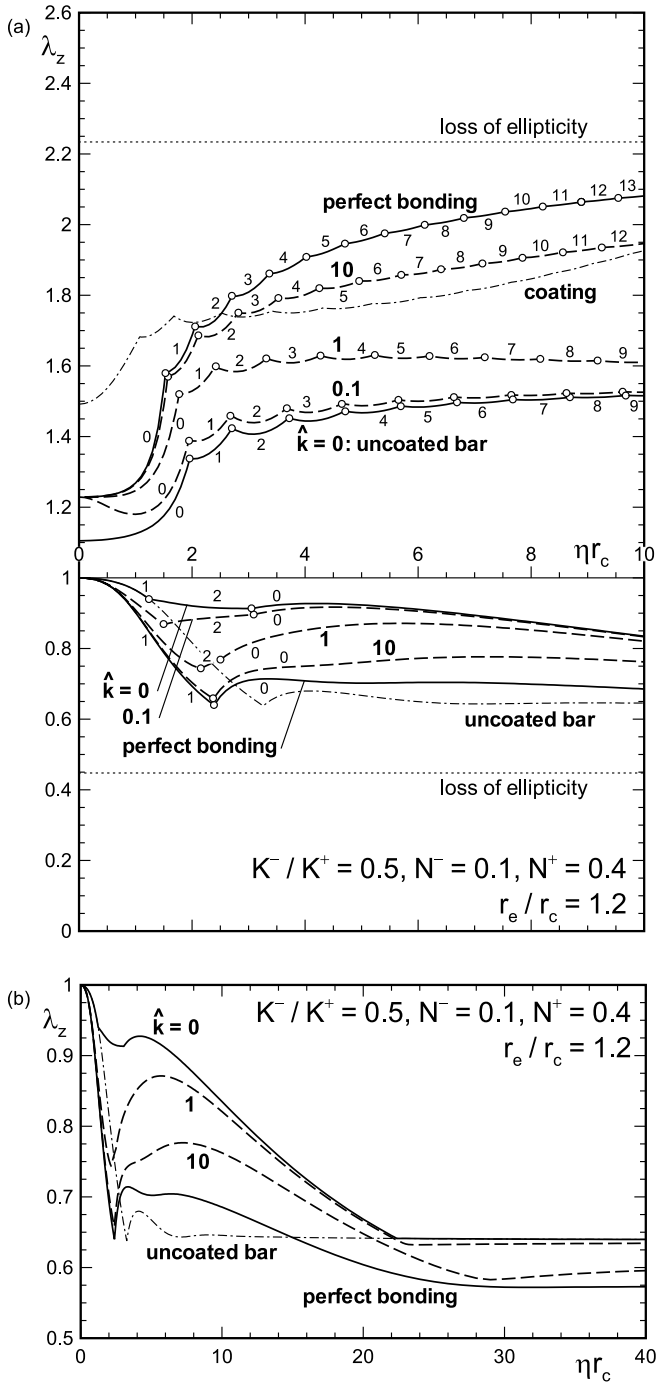

Fig. 6. Axial stretch at bifurcation (λ_z) for a coated elastic cylinder ($r_e/r_c = 1.2$) as a function of the core radius (r_c) multiplied by the bifurcation wave number (η). Various values of interfacial stiffness $\hat{k}$ are considered. A small number close to a curve denotes the critical circumferential mode, changing in correspondence of a spot on the curve. The coating and the core are both J_2-deformation theory materials with $K^-/K^+ = 0.5$, $N^- = 0.1$ and $N^+ = 0.4$. (a) $\eta r_c \leqslant 10$. (b) $\eta r_c \leqslant 40$.

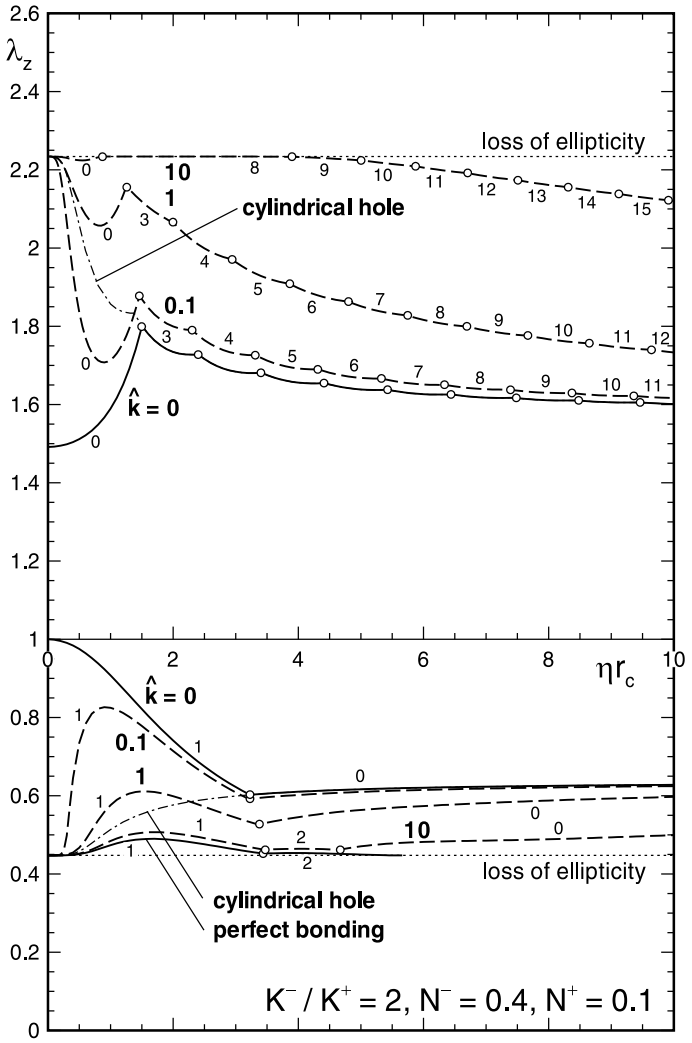

Fig. 7. Axial stretch at bifurcation (λ_z) for an elastic cylinder embedded in an infinite elastic matrix as a function of the core radius (r_c) multiplied by the bifurcation wave number (η). Various values of interfacial stiffness $\hat{k}$ are considered. A small number close to a curve denotes the critical circumferential mode, changing in correspondence of a spot on the curve. The coating and the matrix are both J_2-deformation theory materials with $K^-/K^+ = 2$, $N^- = 0.4$ and $N^+ = 0.1$.

circumferential modes become available; for instance, the mode $n = 3$ starts to be critical for an elastic tube with $r_e/r_c < 1.14$.

The situation where the coating is stiffer than the core ($\mu^-/\mu^+ = 0.1$) is reported in Fig. 2(b). Here the bifurcation behaviour is strongly conditioned by the external coating and the critical stretches referred to the two limiting cases of perfect bonding and complete separation set a narrow zone in which all curves lie. In contrast to Fig. 2(a), all curves in Fig. 2(b) exhibit a range where the circumferential mode $n = 2$ is critical. For perfectly bonded interface, the curve $r_e/r_c = 1.2$ of Fig. 1(b) is recovered while, for $\hat{k} = 0$, the same results reported in Fig. 2(a) are obtained. Similarly to the part (a) of this figure, the bifurcation stretches of the inner bar are plotted for comparison (labelled as 'uncoated bar'). A calculation of the total

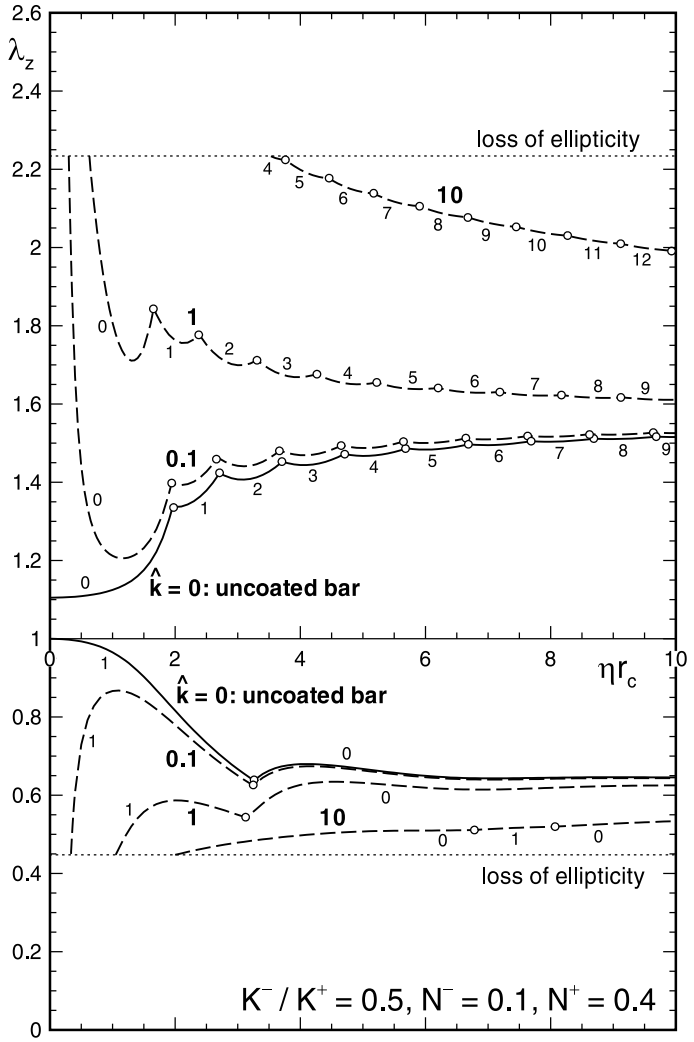

Fig. 8. Axial stretch at bifurcation (λ_z) for an elastic cylinder embedded in an infinite elastic matrix as a function of the core radius (r_c) multiplied by the bifurcation wave number (η). Various values of interfacial stiffness $\hat{k}$ are considered. A small number close to a curve denotes the critical circumferential mode, changing in correspondence of a spot on the curve. The coating and the matrix are both J_2-deformation theory materials with $K^-/K^+ = 0.5$, $N^- = 0.1$ and $N^+ = 0.4$.

axial loads relative to the cases of perfect bonding and isolated core reveals that the total load at bifurcation of the coated bar is always higher than that of the inner bar for all longitudinal modes. At $\eta r_c \approx 6$ the ratio between these total loads approaches a minimum, equal to 1.46.

It is clear from Fig. 2 that at low values of ηr_c (high longitudinal wavelengths) the bifurcation behaviour of the structure is controlled by the core, while for higher values of ηr_c the coating dominates the behaviour. This trend becomes more evident as the interfacial stiffness decreases.

A general conclusion already emerges from Fig. 2. Generally, a decrease in the interfacial stiffness yields a pronounced increase in critical stretch and, in a sense, the interfacial compliance produces curves 'intermediate' to the perfectly bonded and complete separation cases.

Fig. 3 is relative to the case in which the coating becomes infinitely thick, representative of a fiber embedded in a matrix. In part (a) of the figure the inner core is stiffer than the matrix ($\mu^-/\mu^+ = 10$) and the bifurcation behaviour of the structure is dominated by the stiffer material for all values of interfacial stiffness. Only antisymmetric and axisymmetric modes are involved in all cases. The transition between them occurs always when $\eta r_c > 10$. For non-vanishing interfacial stiffness, a dominant wavelength can be recognized, corresponding to a buckling-like mode of the inner cylinder. Moreover, with the exception of the complete separation case $\hat{k} = 0$, the limit $\eta r_c \to 0$ can be viewed as the vanishing of the radius of the bar. This corresponds to a situation where an infinite layer is compressed at its opposite faces, a case in which bifurcation is not found. For this reason, all curves of Fig. 3 with $\hat{k} \neq 0$ approach the infinite compression limit $\lambda_z = 0$ when $\eta r_c \to 0$.

In the case of complete separation between fiber and matrix ($\hat{k} = 0$), critical stretches are those relative to the bar for $\eta r_c \leqslant 10.30$ (antisymmetric mode) and for $\eta r_c > 14.27$ (axisymmetric mode, labelled as '0(b)' in the particular of Fig. 3(a)). For $10.30 < \eta r_c \leqslant 14.27$ the matrix with the cylindrical hole sets the critical stretch for bifurcation with an axisymmetric mode (labelled as '0(ch)'). Note that the entire curve relative to a cylindrical hole in a matrix is also reported in the figure. Another interesting detail is that the curve relative to the case of perfectly bonded interface approaches the interfacial instability, $\lambda_z \approx 0.392$, in the small wavelength limit $\eta r_c \to \infty$, while the other curves tend to the surface instability of the cylindrical core.

The bifurcation behaviour of a soft bar embedded in a stiffer matrix is reported in Fig. 3(b). The interfacial compliance plays here an important role, particularly at high longitudinal wavelengths. For sufficiently small values of $\hat{k}$ a dominant wavelength develops as in Fig. 3(a), but for stiff interfaces this does not occur. When the two bodies are completely separated the critical stretches of Fig. 3(a) are recovered.

4.2. J_2-deformation theory of plasticity

As will become evident soon, the behaviour for J_2-deformation theory of plasticity turns out to be much more complicated than for the Mooney–Rivlin case. In particular, the constitutive assumptions of the J_2-deformation theory of plasticity allow the possibility of a variety of bifurcation modes, including necking in tension and loss of ellipticity in tension and compression. Within the elliptic region, in which diffuse bifurcation modes are sought, and with the restrictions on the hardening exponent N $(0 < N \leqslant 1)$, the regime is always (EC). The uniaxial stress–strain law is $\sigma = K\varepsilon_e^{N-1} \ln \lambda_z$. Loss of ellipticity occurs at (EC)/H boundary at a strain level corresponding to values of λ_z satisfying

$$\left(\frac{3 \ln \lambda_z}{3N+1}\right)^2 = \frac{6 \ln \lambda_z}{3N+1} \frac{\lambda_z^3 + 1}{\lambda_z^3 - 1} - 1, \qquad \left|\frac{\ln \lambda_z}{3N+1}\right| > \frac{1}{3}. \tag{71}$$

Only two values of N will be considered, namely, 0.1 and 0.4. For $N = 0.1$ loss of ellipticity occurs at $\lambda_z \approx 0.448$ in compression and $\lambda_z \approx 2.234$ in tension, while for $N = 0.4$ it occurs at $\lambda_z \approx 0.337$ and $\lambda_z \approx 2.972$. Failure of ellipticity will be denoted by a dotted, horizontal line in all following figures.

Fig. 4 has been reported by way of illustration. It pertains to the case of an isolated elastic cylinder with $N = 0.1$ and $N = 0.4$. In the latter case, the complete curves of critical stretch for bifurcation have been reported, for different modes n ranging between $n = 0$ and $n = 11$. The dashed parts of the curves are not attainable in a continuous deformation path starting from an unloaded configuration. In the former case, $N = 0.1$, only the critical curves have been reported.

Let us focus on the $N = 0.4$ case, starting from the behaviour in compression. Critical stretches correspond to the antisymmetric mode at high longitudinal wavelengths ($\eta r_c < 3.78$) and to the axisymmetric mode for $\eta r_c \geqslant 4.53$. There is also a small range where the mode $n = 2$ becomes critical. As expected,

bifurcation occurs at $\lambda_z = 1$, corresponding to $\sigma = 0$, in the long wavelength limit $\eta r_c = 0$. Close to $\eta r_c = 0$ the cylinder bifurcates in an Euler buckling mode. In the short longitudinal wavelength limit a surface instability corresponding to an incremental plane strain mode (similar to that observed for the Mooney–Rivlin material) is found at $\lambda_z \approx 0.572$. With a generic N the critical stretches in tension and compression are, for surface instability, the solutions of the equation (Bassani et al., 1980; Hutchinson and Tvergaard, 1980)

$$3(1 - \lambda_z^{-3/2}) \ln \lambda_z = 3N + 1. \tag{72}$$

Let us now analyze tension. Here all circumferential modes are involved in giving the critical stretch in some range. In particular, for $\eta r_c = 0$ the condition for the necking instability is recovered. This occurs at the maximum load point, when the true stress σ equals the tangent modulus $3\mu_1$ yielding $\lambda_z = \exp(N)$ for the J_2-deformation theory solid. The axisymmetric mode dominates in the range of ηr_c between 0 and approximately 1.63, after which the mode $n = 1$ prevails. If we continue to follow the curve corresponding to the axisymmetric mode $n = 0$, we find that the critical stretch increases and approaches, for high longitudinal frequencies $\eta r_c \to \infty$, the surface instability limit corresponding to the root of Eq. (72) in tension (for $N = 0.4$ this is $\lambda_z \approx 2.614$). This occurs with all individual curves relative to the different modes n. However, the global bifurcation behaviour is determined by the lower envelope of these curves. In this way, the actual small-wavelength bifurcation limit reached by the bar in tension is not an incremental plane strain field, rather, it involves a circumferential wave mode (Hutchinson and Tvergaard, 1980). This occurs at $\lambda_z \approx 2.14$ (for $N = 0.4$) and corresponds to the 'orange peel' pattern experimentally observed by Rittel and Roman (1989), Rittel (1990) and Rittel et al. (1991).

The case $N = 0.1$ is similar to the case $N = 0.4$, with the difference, in compression, that only antisymmetric and axisymmetric modes set the critical stretches. From Eq. (72) the surface instability limit in compression corresponds to $\lambda_z \approx 0.638$, while the curve of bifurcation tends to the value $\lambda_z \approx 1.56$ in tension.

Figs. 5 and 6 pertain to the coated cylinder, with $r_e/r_c = 1.2$. This is investigated for various values of interfacial stiffness $\hat{k}$. Solutions relative to the isolated coating and core are reported in both figures, for comparison.

The results reported in Fig. 5 are relative to $K^-/K^+ = 2$, $N^- = 0.4$ and $N^+ = 0.1$, so that the coating is weaker than the core. Let us focus first on the behaviour in compression and follow the curves with increasing $\hat{k}$. In the case of complete separation ($\hat{k} = 0$), the bifurcation stretches are always set by the coating. For $\eta r_c < 0.76$ the critical mode is the antisymmetric, while for $0.76 \leqslant \eta r_c < 2.35$ and $\eta r_c > 2.35$ the critical modes are $n = 2$ and $n = 0$, respectively. The curves relative to $\hat{k} = 0.1$, $\hat{k} = 1$ and $\hat{k} = 10$ exhibit the same succession of critical circumferential modes and their overall trend is similar to that reported in Fig. 2 for the Mooney–Rivlin material. In particular, for high longitudinal wavelengths, the coated cylinder follows the behaviour of the inner bar, whereas the coating dictates the bifurcations in the short wavelengths range. Moreover, all curves in the figure (with the exception of the case 'uncoated bar') approach the surface instability limit of the external coating, $\lambda_z \approx 0.638$, as $\eta r_c \to \infty$. For a perfectly bonded interface, the antisymmetric mode prevails when $\eta r_c < 3.22$, then the mode $n = 2$ becomes critical, for $3.22 \leqslant \eta r_c < 5.16$. In the range $5.16 \leqslant \eta r_c < 12.75$, eight modes follow one upon the other, i.e. $n = 0$, 3, 0, 4, 5, 6, 7, 8 (the latter two modes fall outside the range of the figure). The mode for $\eta r_c = 10$ is $n = 5$. The curve attains a minimum outside the range of the figure, at $\eta r_c \approx 11.34$ ($\lambda_z \approx 0.479$, greater than the loss of ellipticity of the coating). Moreover, for $\eta r_c \geqslant 12.75$ the axisymmetric mode prevails again, approaching the surface instability ($\lambda_z \approx 0.638$) as the other cases do. Further analyses (not reported) show that this particular trend becomes more evident as the ratio N^-/N^+ increases.

In the tension range, all curves show the typical behaviour described for the cylindrical bar, i.e. the critical circumferential mode increases with a regular succession as ηr_c increases. A necking-type instability at $\eta r_c = 0$ involving core and coating is met at a strain level corresponding to $\lambda_z \approx 1.390$, independently of the value of interfacial stiffness $\hat{k}$. When the interfacial compliance becomes high, the curve of the isolated

coating is approached. This curve sets the lower bifurcation stretch in the case of complete separation between core and coating. All curves approach the surface instability limit for the coating ($\lambda_z \approx 1.56$) as $\eta r_c \to \infty$. The bifurcation stretches of the uncoated bar ($N^- = 0.4$) are plotted for comparison. These closely follow the curve relative to the perfectly bonded interface (at least for $\eta r_c < 4.5$) in compression, whereas in tension there is a remarkable gap between the two curves when $\eta r_c \to 0$ and for short longitudinal wavelengths. However, the total load at necking for the coated structure is approximately 1.21 times greater than that for the uncoated bar, while the same ratio falls to 1.03 for the surface instability limit. It is clear from Fig. 5 that an increase in the interfacial compliance precipitates the solution on the case corresponding to the isolated coating, i.e. to the case pertaining to a hollow cylinder.

Fig. 6 refers to a situation where the coating is stiffer than the core, with constitutive parameters $K^-/K^+ = 0.5$, $N^- = 0.1$ and $N^+ = 0.4$. In compression, now, the isolated coating does not dominates bifurcation for all values of ηr_c when $\hat{k} = 0$, but for $\eta r_c < 1.24$ and for $\eta r_c > 22.38$ the core bifurcates at lower stress than the coating. Indeed, at high longitudinal wavelengths the core ($N^- = 0.1$) attains the limit $\lambda_z \approx 0.638$, whereas the coating ($N^+ = 0.4$) tends to $\lambda_z \approx 0.572$. In Fig. 6(b) the situation for ηr_c up to 40 is reported, to show how the curves behave after the cross point at $\eta r_c \approx 22.38$, $\lambda_z \approx 0.641$. Beyond it, the curves relative to $\hat{k} = 1$ and $\hat{k} = 10$ attain a minimum and then tend to the surface instability of the core, while in the perfect bonding case the surface instability of the coating is approached. It may also be important to note that, differently from Fig. 5, the critical circumferential modes for $\hat{k} = 10$ and perfect bonding are $n = 1$ and $n = 0$ only. In the part of Fig. 6(a) pertaining to tension, the stretch at which necking occurs is $\lambda_z \approx 1.229$, a value intermediate between the isolated coating and the uncoated bar. Here the core sets the minimum stretch at bifurcation in the case of complete separation. Curves relative to the perfect bonding and to $\hat{k} = 10$ intersect the curve relative to the core at $\eta r_c \approx 2.52$ and $\eta r_c \approx 2.77$, respectively.

In all cases, the critical curve is the envelope of several circumferential modes that follow one upon the other as ηr_c increases. In the high longitudinal frequency limit $\eta r_c \to \infty$, curves relative to compliant interfaces approach to the critical value of the uncoated bar ($\lambda_z \approx 1.56$), whereas the limit set by the external coating ($\lambda_z \approx 2.14$) is reached in the perfect bonding case.

Figs. 7 and 8 are relative to the elastic cylinder embedded in an infinite elastic matrix. The core is stiffer than the external medium ($K^-/K^+ = 2$, $N^- = 0.4$ and $N^+ = 0.1$) in Fig. 7, whereas the opposite situation occurs in the case of Fig. 8, where $K^-/K^+ = 0.5$, $N^- = 0.1$ and $N^+ = 0.4$.

In the part of Fig. 7 relative to compression, the effect of the interfacial compliance is strong, particularly at low values of ηr_c, where a dominant longitudinal wavelength comes into play as the interfacial stiffness decreases. This corresponds to a buckling-like mode for the core. When $\hat{k} = 0$ the bifurcation stretch is set by the inner bar for $\eta r_c \leqslant 3.23$ ($n = 1$) and by the matrix with a cylindrical hole for $\eta r_c > 3.23$. The whole curve for this case, which always coincides with the axisymmetric case, is reported in the figure. At $\eta r_c = 0$ all curves with $\hat{k} \neq 0$ approach the loss of ellipticity limit of the matrix, $\lambda_z \approx 0.448$. The same feature occurs also in tension, where the matrix approaches the (EC)/H boundary at $\lambda_z \approx 2.234$. In this part of the diagram, the axisymmetric mode is always the first available at low values of ηr_c. This is immediately followed by $n = 3$ for $\hat{k} = 0, 0.1, 1$ and by $n = 8$ for $\hat{k} = 10$. In the latter case, the mode $n = 8$ is very close to the loss of ellipticity threshold in the range $0.87 < \eta r_c < 3.5$. In all four cases, the critical circumferential mode n increases regularly as ηr_c increases, approaching the surface instability limit of the matrix, $\lambda_z \approx 1.56$. When the fiber and the matrix are perfectly bonded, diffuse bifurcations occur only in compression for $\eta r_c < 5.66$, involving modes $n = 1$ and $n = 2$. Beyond $\eta r_c = 5.66$ strain localization terminates the homogeneous response of the structure. In tension this phenomenon always precedes diffuse modes so that the curve relative to perfect bonding is not reported.

In Fig. 8, the case $\hat{k} = 0$ always corresponds to bifurcation stretches of the uncoated bar. For low values of ηr_c loss of ellipticity in the matrix precedes diffuse bifurcation modes for every value of interfacial compliance. In compression, only axisymmetric and antisymmetric modes are involved.

5. Conclusions

A specific bifurcation problem in velocities has been analyzed, namely, a coated elastic cylinder of circular cross section, subject to uniform stretch with one Eulerian axis coaxial to the axis of cylinder. Effects of several features have been explored, as related to:

- complexity of constitutive equations;
- sign of the current stress (tensile or compressive);
- presence of imperfect bonding at the interface;
- relative (to the core diameter and stiffness) thickness and stiffness of the coating.

All the above features have been found to play important roles in determining the bifurcation thresholds and modes. Particularly for the case of J_2-deformation theory material, the bifurcation modes describe rich geometrical patterns, comprised shear banding, surface and interfacial instabilities, Euler buckling, and high frequency azimuthal modes. From experimental point of view, a variety of modes in axially-loaded structures are known to occur, including parallel wrinkles and 'orange-peel' in metal bars (Rittel, 1990; Rittel et al., 1991), buckled modes, shear bands and microcracks of anodic coatings on aluminium substrates (Block, 1970; Mehdizadeh and Block, 1972), axisymmetric patterns in silicone–rubber cylindrical shells with foam cores (Karam and Gibson, 1995), surface exfoliations in boreholes (Vardoulakis and Sulem, 1995), short wavelength patterns in steel tubes filled with aluminium foam (Seitzberger et al., 1997) Results of this article suggest that the combined effect of geometry, interfacial conditions and complexity of constitutive laws may describe the above-mentioned bifurcation patterns.

Acknowledgements

D.B. gratefully acknowledges financial support of Italian CNR (Contr. n. 97.00466.CT11). M.G. thanks support from University of Trento, Trento, Italy.

Appendix A. Model of interface

We consider two continuous bodies (denoted by indices + and −) that, in the reference configuration, are in contact through an orientable and smooth surface Ξ (Fig. 9). Material points in the Euclidean three-dimensional space are labelled by $\mathbf{x}_0$, so that the current configurations of the two bodies are defined by the deformations

$$\boldsymbol{\chi}^+ : \mathscr{B}_0^+ \to \mathscr{B}^+, \quad \mathbf{x}^+ = \boldsymbol{\chi}^+(\mathbf{x}_0^+), \qquad \boldsymbol{\chi}^- : \mathscr{B}_0^- \to \mathscr{B}^-, \quad \mathbf{x}^- = \boldsymbol{\chi}^-(\mathbf{x}_0^-). \tag{A.1}$$

Let us assume, for the moment, that the two bodies separate during deformation. The contact area Ξ splits into two current areas ξ^+ and ξ^-. In particular, let us consider two spatial points $\mathbf{x}^+ \in \xi^+$ and $\mathbf{x}^- \in \xi^-$ corresponding to the same material point $\mathbf{x}_0^+ = \mathbf{x}_0^- \in \Xi$. At these points, the outward normals and the area elements will be different in general. The Nanson's formula implies

$$\mathbf{n}_0^- \, \mathrm{d}a_0 = J_-^{-1}(\mathbf{F}^-)^{\mathrm{T}}\mathbf{n}^- \, \mathrm{d}a^- = -J_+^{-1}(\mathbf{F}^+)^{\mathrm{T}}\mathbf{n}^+ \, \mathrm{d}a^+, \tag{A.2}$$

where $\mathrm{d}a_0$ and $\mathbf{n}_0^-$ are the area element and the unit normal to Ξ^- (directed away from −) in the reference configuration. The unit vectors $\mathbf{n}^+$ and $\mathbf{n}^-$ are the unit outward normals to surfaces ξ^+ and ξ^-, so that $\mathbf{n}^-$ and $\mathbf{n}^+$ map back to $\mathbf{n}_0^-$ and $\mathbf{n}_0^+ = -\mathbf{n}_0^-$ in the reference configuration.

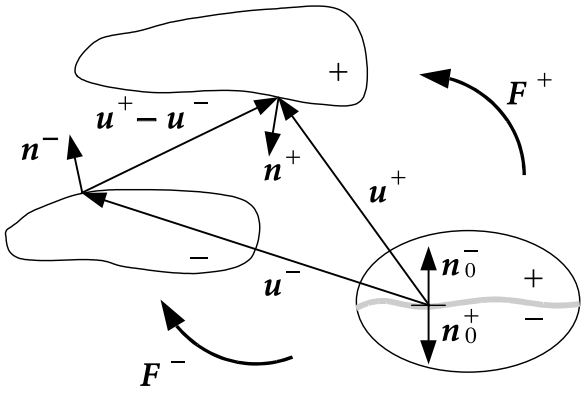

Fig. 9. Kinematics of finite deformation of two bodies in contact in the reference configuration through a linear interface.

We assume that the two surfaces ξ^+ and ξ^- are connected with some material able to transmit forces, such as a glue. Therefore, we assume that, with reference to the above two points, the resultant forces are equal and opposite, and then

$$\mathbf{T}^+\mathbf{n}^+ \,\mathrm{d}a^+ = -\mathbf{T}^-\mathbf{n}^- \,\mathrm{d}a^-, \tag{A.3}$$

and in terms of the first Piola–Kirchhoff stress tensor $\mathbf{S}$:

$$\mathbf{S}^+\mathbf{n}_0^+ = -\mathbf{S}^-\mathbf{n}_0^-, \tag{A.4}$$

where putting $\mathbf{e}_r = \mathbf{n}_0^- = -\mathbf{n}_0^+$ and taking the material time derivative, Eq. (4) is obtained. Moreover, we introduce a constitutive equation for the interface where the resultant force at the two corresponding points is related to the distance between these points:

$$\mathbf{S}^-\mathbf{n}_0^- = k(\mathbf{u}^+ - \mathbf{u}^-), \tag{A.5}$$

which, taking the material time derivative (with $\mathbf{e}_r = \mathbf{n}_0^- = -\mathbf{n}_0^+$) and using Eq. (4), becomes Eq. (6). Parameter k has dimension [stress/length] and represents a strictly positive interfacial stiffness, assumed constant for simplicity. It should be noted that Eq. (A.5) implies that the stress transmitted across the interface vanishes when the jump in displacement is null. Moreover, the two limit cases $k = 0$ and $k \to \infty$ describe the two relevant situations of perfect separation and perfectly bonded interface, respectively. The constitutive equation (A.5) must satisfy two essential requisites:

- it must be invariant with respect to the permutation $+ \leftrightarrow -$;
- it must satisfy the principle of material frame indifference.

The first requirement is evidently met, because a permutation $+$ and $-$ gives

$$\mathbf{S}^+\mathbf{n}_0^+ = -k(\mathbf{u}^+ - \mathbf{u}^-), \tag{A.6}$$

which is fully consistent with Eq. (A.4).

The second requirement needs more attention, and will be explained assuming, for the moment, a more complicated form of Eq. (A.5) where k is replaced by a second-order constitutive tensor $\mathbf{K}$

$$\mathbf{S}^-\mathbf{n}_0^- = \mathbf{K}(\mathbf{u}^+ - \mathbf{u}^-). \tag{A.7}$$

Let us consider two motions $\boldsymbol{\chi}(\mathbf{x}_0, t)$ and $\boldsymbol{\chi}^*(\mathbf{x}_0, t)$ related by a change in observer

$$\mathbf{x}^* = \mathbf{q}(t) + \mathbf{Q}(t)(\mathbf{x} - \mathbf{o}), \tag{A.8}$$

where $\mathbf{q}(t)$, $\mathbf{o}$ and $\mathbf{Q}(t)$ are two points and a rotation, respectively. From Eq. (A.8) the transformation laws can be obtained for first Piola–Kirchhoff stress $\mathbf{S}$, unit normal $\mathbf{n}_0$ and difference in displacements between any two points $\mathbf{u}(\mathbf{x}_0^a, t) - \mathbf{u}(\mathbf{x}_0^b, t)$:

$$\mathbf{S}^* = \mathbf{QS}, \tag{A.9a}$$

$$\mathbf{n}_0^* = \mathbf{n}_0, \tag{A.9b}$$

$$\mathbf{u}^*(\mathbf{x}_0^a, t) - \mathbf{u}^*(\mathbf{x}_0^b, t) + \mathbf{x}_0^b - \mathbf{x}_0^a = \mathbf{Q}[\mathbf{u}(\mathbf{x}_0^b, t) - \mathbf{u}(\mathbf{x}_0^a, t) + \mathbf{x}_0^b - \mathbf{x}_0^a]. \tag{A.9c}$$

For points on the interface $\mathbf{x}_0^a = \mathbf{x}_0^b = \mathbf{x}_0$, (A.9c) becomes

$$(\mathbf{u}^+ - \mathbf{u}^-)^* = \mathbf{Q}(\mathbf{u}^+ - \mathbf{u}^-), \tag{A.10}$$

and therefore the requirement that the *interfacial response be independent of the observer* implies the following transformation rule for the interfacial stiffness tensor $\mathbf{K}$:

$$\mathbf{K}^* = \mathbf{QKQ}^{\mathrm{T}}. \tag{A.11}$$

Obviously, Eq. (A.11) is satisfied in the simple situation Eq. (A.5), where $\mathbf{K} = k\mathbf{I}$.

More generally, using Eq. (A.7) instead of Eq. (A.5) to obtain the incremental interfacial constitutive equations, we get

$$\dot{\mathbf{S}}^- \mathbf{n}_0^- = \dot{\mathbf{K}}(\mathbf{u}^+ - \mathbf{u}^-) + \mathbf{K}(\mathbf{v}^+ - \mathbf{v}^-). \tag{A.12}$$

In the case investigated in this paper, as well as in (Bigoni et al., 1997), the transversal stress in the fundamental path is null, so that $\mathbf{u}^+ - \mathbf{u}^- = \mathbf{0}$ and thus Eq. (A.12) simplifies to

$$\dot{\mathbf{S}}^- \mathbf{n}_0^- = \mathbf{K}(\mathbf{v}^+ - \mathbf{v}^-), \tag{A.13}$$

which is the interfacial constitutive law employed by Bigoni et al. (1997).

If the two surfaces do not separate, a unilateral contact condition should be imposed at Ξ to prohibit interpenetration of the two bodies in contact. This yields nonlinear incremental equations. In the problem analyzed in the present paper, the rate equations (6) are employed to hold incrementally from a state in which $\mathbf{u}^+ - \mathbf{u}^- = \mathbf{0}$. Therefore, in the interest of simplicity, interpenetration may be admitted as an approximation, which might be physically motivated by a non-zero initial thickness of the interface.

Appendix B. Incremental constitutive law

Taking the material time derivative of Eq. (13), we obtain

$$\dot{\mathbf{T}} = -\dot{\pi}\mathbf{I} + \alpha_1 \dot{\mathbf{B}} + \alpha_{-1}(\mathbf{B}^{-1})^{\cdot} + \dot{\alpha}_1 \mathbf{B} + \dot{\alpha}_{-1}\mathbf{B}^{-1}, \tag{B.1}$$

where

$$\dot{\mathbf{B}} = \mathbf{LB} + \mathbf{BL}^{\mathrm{T}}, \tag{B.2a}$$

$$(\mathbf{B}^{-1})^{\cdot} = -(\mathbf{B}^{-1}\mathbf{L} + \mathbf{L}^{\mathrm{T}}\mathbf{B}^{-1}). \tag{B.2b}$$

Using the definition of Jaumann derivative

$$\overset{\nabla}{\mathbf{T}} = \dot{\mathbf{T}} - \mathbf{WT} + \mathbf{TW},$$

where $\mathbf{W}$ is the spin, it follows that

$$\overset{\nabla}{\mathbf{T}} = -\dot{\pi}\mathbf{I} + \alpha_1(\mathbf{BD}+\mathbf{DB}) - \alpha_{-1}(\mathbf{B}^{-1}\mathbf{D}+\mathbf{DB}^{-1}) + \dot{\alpha}_1\mathbf{B} + \dot{\alpha}_{-1}\mathbf{B}^{-1}. \tag{B.3}$$

Employing the identity $\overset{\nabla}{p} = \mathrm{tr}\overset{\nabla}{\mathbf{T}}/3$, the Lagrange multiplier $\dot{\pi}$ can be eliminated, then

$$\overset{\nabla}{\mathbf{T}} = \overset{\nabla}{p}\mathbf{I} + \alpha_1(\mathbf{BD}+\mathbf{DB})_{\mathrm{dev}} - \alpha_{-1}(\mathbf{B}^{-1}\mathbf{D}+\mathbf{DB}^{-1})_{\mathrm{dev}} + \dot{\alpha}_1(\mathbf{B})_{\mathrm{dev}} + \dot{\alpha}_{-1}(\mathbf{B}^{-1})_{\mathrm{dev}}, \tag{B.4}$$

where $(\mathbf{A})_{\mathrm{dev}} = \mathbf{A} - (\mathrm{tr}\mathbf{A}/3)\mathbf{I}$ denotes the deviatoric part of any second-order tensor $\mathbf{A}$. Moreover, due to the incompressibility constraint, the material time derivatives of functions α_1 and α_{-1} can be obtained in the useful form

$$\dot{\alpha}_m = \frac{\partial\alpha_m}{\partial\lambda_1}\dot{\lambda}_1 + \frac{\partial\alpha_m}{\partial\lambda_2}\dot{\lambda}_2 \quad (m = 1, -1), \tag{B.5}$$

and, using the spectral decomposition of the left Cauchy–Green strain tensor with $\mathbf{b}_i$ $(i = 1, 2, 3)$ denoting the Eulerian principal axes, we may express the material time derivative of the principal stretches as functions of $\dot{\mathbf{B}}$, i.e.

$$\dot{\lambda}_1 = \frac{1}{2\lambda_1}\mathbf{b}_1\cdot\dot{\mathbf{B}}\mathbf{b}_1, \qquad \dot{\lambda}_2 = \frac{1}{2\lambda_2}\mathbf{b}_2\cdot\dot{\mathbf{B}}\mathbf{b}_2. \tag{B.6}$$

By employing now Eq. (B.2a), we may rewrite (B.5) in terms of the Eulerian strain rate $\mathbf{D}$

$$\dot{\alpha}_m = \left(\frac{\partial\alpha_m}{\partial\lambda_1}\lambda_1\mathbf{b}_1\otimes\mathbf{b}_1 + \frac{\partial\alpha_m}{\partial\lambda_2}\lambda_2\mathbf{b}_2\otimes\mathbf{b}_2\right)\cdot\mathbf{D} \quad (m = 1, -1). \tag{B.7}$$

For axisymmetric geometry $\lambda_1 = \lambda_z$ and $\lambda_2 = \lambda_3 = \lambda_z^{-1/2}$, so that $\alpha_1 = \alpha_1(\lambda_z)$ and $\alpha_{-1} = \alpha_{-1}(\lambda_z)$. With $\mathbf{G} = \mathbf{e}_z\otimes\mathbf{e}_z$, the tensors $\mathbf{B}$ and $\mathbf{B}^{-1}$ take the following form

$$\mathbf{B} = \left(\lambda_z^2 - \frac{1}{\lambda_z}\right)\mathbf{G} + \frac{1}{\lambda_z}\mathbf{I}, \qquad \mathbf{B}^{-1} = \left(\frac{1}{\lambda_z^2} - \lambda_z\right)\mathbf{G} + \lambda_z\mathbf{I}. \tag{B.8}$$

In addition, we have the equations

$$\dot{\lambda}_z = \frac{1}{2\lambda_z}\mathbf{e}_z\cdot\dot{\mathbf{B}}\mathbf{e}_z, \qquad \dot{\alpha}_m = \frac{\mathrm{d}\alpha_m}{\mathrm{d}\lambda_z}\lambda_z\mathbf{G}\cdot\mathbf{D} \quad (m = 1, -1). \tag{B.9}$$

As a conclusion, Eq. (B.4) can be written in the axisymmetric case in the form (8) and (9).

Appendix C. Elements of $[M^{C}]$, $[M^{M,EI}]$ and $[M^{M,EC}]$

Let us introduce the functions

$$J_*(\rho_j, x, y, r) = x^-(r)J_n(\rho_j^-\eta r) + y^-(r)\rho_j^-\eta r J_{n+1}(\rho_j^-\eta r), \tag{C.1}$$

$$I_*^{\mp}(x, y, r) = x^{\mp}(r)I_n(\rho_3^{\mp}\eta r) + y^{\mp}(r)\rho_3^{\mp}\eta r I_{n+1}(\rho_3^{\mp}\eta r), \tag{C.2}$$

$$H_*^{(i)}(\rho_j, x, y, r) = x^+(r)H_n^{(i)}(\rho_j^+\eta r) + y^+(r)\rho_j^+\eta r H_{n+1}^{(i)}(\rho_j^+\eta r) \quad (i = 1, 2), \tag{C.3}$$

$$K_*(x, y, r) = x^+(r)K_n(\rho_3^+\eta r) + y^+(r)\rho_3^+\eta r K_{n+1}(\rho_3^+\eta r). \tag{C.4}$$

By definition, $J_*(\rho_j, x, y, r)$ is relative to the inner cylindrical core only, whereas $H_*^{(i)}(\rho_j, x, y, r)$ $(i = 1, 2)$ and $K_*(x, y, r)$ are defined only for the coating. The function $I_*^{\mp}(x, y, r)$ is relative to both bodies and the relevant superscript has to be considered.

The elements of the matrices $[M^{\mathrm{C}}]$, $[M^{\mathrm{M,EI}}]$ and $[M^{\mathrm{M,EC}}]$ in Eqs. (66) and (70) are:

$$
\begin{aligned}
&M^{\mathrm{C}}_{1j} = M^{\mathrm{M,EI}}_{1j} = M^{\mathrm{M,EC}}_{1j} = J_*(\rho_j, F_1(r_\mathrm{c}), 2\hat{E}, r_\mathrm{c}) \quad (j=1,2),\\
&M^{\mathrm{C}}_{13} = M^{\mathrm{M,EI}}_{13} = M^{\mathrm{M,EC}}_{13} = 2n\hat{E}^- I^-_*(n-1,1,r_\mathrm{c}),\\
&M^{\mathrm{C}}_{14} = M^{\mathrm{M,EI}}_{14} = M^{\mathrm{M,EC}}_{14} = -\hat{\mu} H^{(1)}_*(\rho_1, F_1(r_\mathrm{c}), 2\hat{E}, r_\mathrm{c}),\\
&M^{\mathrm{C}}_{15} = M^{\mathrm{M,EI}}_{15} = -\hat{\mu} H^{(1)}_*(\rho_2, F_2(r_\mathrm{c}), 2\hat{E}, r_\mathrm{c}),\\
&M^{\mathrm{C}}_{16} = -\hat{\mu} H^{(2)}_*(\rho_1, F_1(r_\mathrm{c}), 2\hat{E}, r_\mathrm{c}),\\
&M^{\mathrm{C}}_{17} = M^{\mathrm{M,EC}}_{15} = -\hat{\mu} H^{(2)}_*(\rho_2, F_2(r_\mathrm{c}), 2\hat{E}, r_\mathrm{c}),\\
&M^{\mathrm{C}}_{18} = -2n\hat{\mu}\hat{E}^+ I^+_*(n-1,1,r_\mathrm{c}),\\
&M^{\mathrm{C}}_{19} = M^{\mathrm{M,EI}}_{16} = M^{\mathrm{M,EC}}_{16} = -2n\hat{\mu}\hat{E}^+ K_*(n-1,-1,r_\mathrm{c}),
\end{aligned}
$$

$$
\begin{aligned}
&M^{\mathrm{C}}_{2j} = M^{\mathrm{M,EI}}_{2j} = M^{\mathrm{M,EC}}_{2j} = 2n\hat{E}^- J_*(\rho_j, 1-n, 1, r_\mathrm{c}) \quad (j=1,2),\\
&M^{\mathrm{C}}_{23} = M^{\mathrm{M,EI}}_{23} = M^{\mathrm{M,EC}}_{23} = 2\hat{E}^- I^-_*(-G(r_\mathrm{c}), 1, r_\mathrm{c}),\\
&M^{\mathrm{C}}_{24} = M^{\mathrm{M,EI}}_{24} = M^{\mathrm{M,EC}}_{24} = -2n\hat{\mu}\hat{E}^+ H^{(1)}_*(\rho_1, 1-n, 1, r_\mathrm{c}),\\
&M^{\mathrm{C}}_{25} = M^{\mathrm{M,EI}}_{25} = -2n\hat{\mu}\hat{E}^+ H^{(1)}_*(\rho_2, 1-n, 1, r_\mathrm{c}),\\
&M^{\mathrm{C}}_{26} = -2n\hat{\mu}\hat{E}^+ H^{(2)}_*(\rho_1, 1-n, 1, r_\mathrm{c}),\\
&M^{\mathrm{C}}_{27} = M^{\mathrm{M,EC}}_{25} = -2n\hat{\mu}\hat{E}^+ H^{(2)}_*(\rho_2, 1-n, 1, r_\mathrm{c}),\\
&M^{\mathrm{C}}_{28} = 2\hat{\mu}\hat{E}^+ I^+_*(G(r_\mathrm{c}), -1, r_\mathrm{c}),\\
&M^{\mathrm{C}}_{29} = M^{\mathrm{M,EI}}_{26} = M^{\mathrm{M,EC}}_{26} = 2\hat{\mu}\hat{E}^+ K_*(G(r_\mathrm{c}), 1, r_\mathrm{c}),
\end{aligned}
$$

$$
\begin{aligned}
&M^{\mathrm{C}}_{3j} = M^{\mathrm{M,EI}}_{3j} = M^{\mathrm{M,EC}}_{3j} = (\rho_j^{-2}-1)\hat{A}^- J_*(\rho_j, n, -1, r_\mathrm{c}) \quad (j=1,2),\\
&M^{\mathrm{C}}_{33} = M^{\mathrm{M,EI}}_{33} = M^{\mathrm{M,EC}}_{33} = -n\hat{A}^- I^-_*(1,0,r_\mathrm{c}),\\
&M^{\mathrm{C}}_{34} = M^{\mathrm{M,EI}}_{34} = M^{\mathrm{M,EC}}_{34} = -\hat{\mu}(\rho_1^{+2}-1)\hat{A}^+ H^{(1)}_*(\rho_1, n, -1, r_\mathrm{c}),\\
&M^{\mathrm{C}}_{35} = M^{\mathrm{M,EI}}_{35} = -\hat{\mu}(\rho_2^{+2}-1)\hat{A}^+ H^{(1)}_*(\rho_2, n, -1, r_\mathrm{c}),\\
&M^{\mathrm{C}}_{36} = -\hat{\mu}(\rho_1^{+2}-1)\hat{A}^+ H^{(2)}_*(\rho_1, n, -1, r_\mathrm{c}),\\
&M^{\mathrm{C}}_{37} = M^{\mathrm{M,EC}}_{35} = -\hat{\mu}(\rho_2^{+2}-1)\hat{A}^+ H^{(2)}_*(\rho_2, n, -1, r_\mathrm{c}),\\
&M^{\mathrm{C}}_{38} = n\hat{\mu}\hat{A}^+ I^+_*(1,0,r_\mathrm{c}),\\
&M^{\mathrm{C}}_{39} = M^{\mathrm{M,EI}}_{36} = M^{\mathrm{M,EC}}_{36} = n\hat{\mu}\hat{A}^+ K_*(1,0,r_\mathrm{c}),
\end{aligned}
$$

$$
\begin{aligned}
&M^{\mathrm{C}}_{4j} = M^{\mathrm{M,EI}}_{4j} = M^{\mathrm{M,EC}}_{4j} = J_*(\rho_j, F_1(r_\mathrm{c}) + n\hat{k}, 2\hat{E} - \hat{k}, r_\mathrm{c}) \quad (j=1,2),\\
&M^{\mathrm{C}}_{43} = M^{\mathrm{M,EI}}_{43} = M^{\mathrm{M,EC}}_{43} = nI^-_*(2(n-1)\hat{E} + \hat{k}, 2\hat{E}, r_\mathrm{c}),\\
&M^{\mathrm{C}}_{44} = M^{\mathrm{M,EI}}_{44} = M^{\mathrm{M,EC}}_{44} = -\hat{k} H^{(1)}_*(\rho_1, n, -1, r_\mathrm{c}),\\
&M^{\mathrm{C}}_{45} = M^{\mathrm{M,EI}}_{45} = -\hat{k} H^{(1)}_*(\rho_2, n, -1, r_\mathrm{c}),\\
&M^{\mathrm{C}}_{46} = -\hat{k} H^{(2)}_*(\rho_1, n, -1, r_\mathrm{c}),\\
&M^{\mathrm{C}}_{47} = M^{\mathrm{M,EC}}_{45} = -\hat{k} H^{(2)}_*(\rho_2, n, -1, r_\mathrm{c}),\\
&M^{\mathrm{C}}_{48} = -n\hat{k} I^+_*(1,0,r_\mathrm{c}),\\
&M^{\mathrm{C}}_{49} = M^{\mathrm{M,EI}}_{46} = M^{\mathrm{M,EC}}_{46} = -n\hat{k} K_*(1,0,r_\mathrm{c}),
\end{aligned}
$$

$$
\begin{aligned}
&M^{\mathrm{C}}_{5j} = M^{\mathrm{M,EI}}_{5j} = M^{\mathrm{M,EC}}_{5j} = nJ_*(\rho_j, 2(1-n)\hat{E} - \hat{k}, 2\hat{E}, r_\mathrm{c}) \quad (j = 1,2),\\
&M^{\mathrm{C}}_{53} = M^{\mathrm{M,EI}}_{53} = M^{\mathrm{M,EC}}_{53} = I^-_*(-2\hat{E}G(r_\mathrm{c}) - n\hat{k}, 2\hat{E} - \hat{k}, r_\mathrm{c}),\\
&M^{\mathrm{C}}_{54} = M^{\mathrm{M,EI}}_{54} = M^{\mathrm{M,EC}}_{54} = n\hat{k}H^{(1)}_*(\rho_1, 1, 0, r_\mathrm{c}),\\
&M^{\mathrm{C}}_{55} = M^{\mathrm{M,EI}}_{55} = n\hat{k}H^{(1)}_*(\rho_2, 1, 0, r_\mathrm{c}),\\
&M^{\mathrm{C}}_{56} = n\hat{k}H^{(2)}_*(\rho_1, 1, 0, r_\mathrm{c}),\\
&M^{\mathrm{C}}_{57} = M^{\mathrm{M,EC}}_{55} = n\hat{k}H^{(2)}_*(\rho_2, 1, 0, r_\mathrm{c}),\\
&M^{\mathrm{C}}_{58} = \hat{k}I^+_*(n, 1, r_\mathrm{c}),\\
&M^{\mathrm{C}}_{59} = M^{\mathrm{M,EI}}_{56} = M^{\mathrm{M,EC}}_{56} = \hat{k}K^+_*(n, -1, r_\mathrm{c}),
\end{aligned}
$$

$$
\begin{aligned}
&M^{\mathrm{C}}_{6j} = M^{\mathrm{M,EI}}_{6j} = M^{\mathrm{M,EC}}_{6j} = J_*(\rho_j, n(\rho_j^2 - 1)\hat{A} + \rho_j^2\hat{k}, (1-\rho_j^2)\hat{A}, r_\mathrm{c}) \quad (j = 1,2),\\
&M^{\mathrm{C}}_{63} = M^{\mathrm{M,EI}}_{63} = M^{\mathrm{M,EC}}_{63} = -n\hat{A}^- I^-_*(1, 0, r_\mathrm{c}),\\
&M^{\mathrm{C}}_{64} = M^{\mathrm{M,EI}}_{64} = M^{\mathrm{M,EC}}_{64} = -\rho_1^{+2}\hat{k}H^{(1)}_*(\rho_1, 1, 0, r_\mathrm{c}),\\
&M^{\mathrm{C}}_{65} = M^{\mathrm{M,EI}}_{65} = -\rho_2^{+2}\hat{k}H^{(1)}_*(\rho_2, 1, 0, r_\mathrm{c}),\\
&M^{\mathrm{C}}_{66} = -\rho_1^{+2}\hat{k}H^{(2)}_*(\rho_1, 1, 0, r_\mathrm{c}),\\
&M^{\mathrm{C}}_{67} = M^{\mathrm{M,EC}}_{65} = -\rho_2^{+2}\hat{k}H^{(2)}_*(\rho_2, 1, 0, r_\mathrm{c}),\\
&M^{\mathrm{C}}_{68} = 0,\\
&M^{\mathrm{C}}_{69} = M^{\mathrm{M,EI}}_{66} = M^{\mathrm{M,EC}}_{66} = 0,
\end{aligned}
$$

$$
\begin{aligned}
&M^{\mathrm{C}}_{7j} = 0 \quad (j = 1,2,3),\\
&M^{\mathrm{C}}_{7j} = H^{(1)}_*(\rho_{j-3}, F_{j-3}(r_\mathrm{e}), 2\hat{E}, r_\mathrm{e}) \quad (j = 4,5),\\
&M^{\mathrm{C}}_{7j} = H^{(2)}_*(\rho_{j-5}, F_{j-5}(r_\mathrm{e}), 2\hat{E}, r_\mathrm{e}) \quad (j = 6,7),\\
&M^{\mathrm{C}}_{78} = 2n\hat{E}^+ I^+_*(n-1, 1, r_\mathrm{e}),\\
&M^{\mathrm{C}}_{79} = 2n\hat{E}^+ K_*(n-1, -1, r_\mathrm{e}),
\end{aligned}
$$

$$
\begin{aligned}
&M^{\mathrm{C}}_{8j} = 0 \quad (j = 1,2,3),\\
&M^{\mathrm{C}}_{8j} = nH^{(1)}_*(\rho_{j-3}, n-1, -1, r_\mathrm{e}) \quad (j = 4,5),\\
&M^{\mathrm{C}}_{8j} = nH^{(2)}_*(\rho_{j-5}, n-1, -1, r_\mathrm{e}) \quad (j = 6,7),\\
&M^{\mathrm{C}}_{88} = I^+_*(G(r_\mathrm{e}), -1, r_\mathrm{e}),\\
&M^{\mathrm{C}}_{89} = K_*(G(r_\mathrm{e}), 1, r_\mathrm{e}),
\end{aligned}
$$

$$
\begin{aligned}
&M^{\mathrm{C}}_{9j} = 0 \quad (j = 1,2,3),\\
&M^{\mathrm{C}}_{9j} = (\rho_{j-3}^{+2} - 1)H^{(1)}_*(\rho_{j-3}, n, -1, r_\mathrm{e}) \quad (j = 4,5),\\
&M^{\mathrm{C}}_{9j} = (\rho_{j-5}^{+2} - 1)H^{(2)}_*(\rho_{j-5}, n, -1, r_\mathrm{e}) \quad (j = 6,7),\\
&M^{\mathrm{C}}_{98} = -I^+_*(1, 0, r_\mathrm{e}),\\
&M^{\mathrm{C}}_{99} = -K_*(1, 0, r_\mathrm{e}),
\end{aligned}
$$

where

$$F_j^{\mp}(r) = \left\{ 2n(n-1)\hat{E} - \rho_j^2\eta^2 r^2 \left[\rho_j^2 - 1 + 2\,\frac{\mu_1+\mu_2}{\mu_3} - \frac{\sigma}{2\mu_3}(\rho_j^2+1) \right] \right\}^{\mp}, \tag{C.5}$$

$$G^{\mp}(r) = n(n-1) + \frac{1}{2}\rho_3^{\mp 2}\eta^2 r^2, \tag{C.6}$$

$$\hat{k} = \frac{kr_c}{\mu_3^-}, \qquad \hat{E}^{\mp} = \frac{E^{\mp}}{\mu_3^{\mp}}, \qquad \hat{A}^{\mp} = \frac{A^{\mp}}{\mu_3^{\mp}}, \qquad \hat{\mu} = \frac{\mu_3^+}{\mu_3^-}. \tag{C.7}$$

The notation $\{\ \}^{\mp}$ means that all quantities inside braces have to be evaluated according to the superscript.

References

Bassani, J.L., Durban, D., Hutchinson, J.W., 1980. Bifurcation at a spherical hole in an infinite elastoplastic medium. Math. Proc. Camb. Phil. Soc. 87, 339–356.

Bigoni, D., Ortiz, M., Needleman, A., 1997. Effect of interfacial compliance on bifurcation of a layer bonded to a substrate. Int. J. Solids Struct. 34, 4305–4326.

Biot, M.A., 1965. Mechanics of Incremental Deformations. Wiley, New York.

Block, R.J., 1970. Buckling of anodic coatings. J. Electrochem. Soc.: Solid State Sci. Technol. 117, 788–791.

Budiansky, B., 1999. On the minimum weights of compression structures. Int. J. Solids Struct. 36, 3677–3708.

Chau, K.T., 1992. Non-normality and bifurcation in a compressible pressure-sensitive circular cylinder under axisymmetric tension and compression. Int. J. Solids Struct. 29, 801–824.

Chau, K.T., 1995. Buckling, barrelling, and surface instabilities of a finite, transversely isotropic circular cylinder. Quart. Appl. Math. 53, 225–244.

Chau, K.T., Choi, S.K., 1998. Bifurcations of thick-walled hollow cylinders of geomaterials under axisymmetric compression. Int. J. Numer. Anal. Meth. Geomech. 22, 903–919.

Cheng, S.Y., Ariaratnam, S.T., Dubey, R.N., 1971. Axisymmetric bifurcation in an elastic–plastic cylinder under axial load and lateral hydrostatic pressure. Quart. Appl. Math. 29, 41–51.

Davies, P.J., 1991. Buckling and barrelling instabilities of nonlinearly elastic columns. Quart. Appl. Math. 49, 407–426.

Fosdick, R.L., Shield, R.T., 1963. Small bending of a circular bar superposed on finite extension or compression. Arch. Rat. Mech. Anal. 12, 223–248.

Haughton, D.M., Ogden, R.W., 1979. Bifurcation of inflated circular cylinders of elastic material under axial loading-II. Exact theory for thick-walled tubes. J. Mech. Phys. Solids 27, 489–512.

Haughton, D.M., Ogden, R.W., 1980. Bifurcation of finitely deformed rotating elastic cylinders. Quart. J. Mech. Appl. Math. 33, 251–265.

Herrmann, G., Forrestal, M.J., 1965. Buckling of a long cylindrical shell containing an elastic core. AIAA J. 3, 1710–1715.

Hill, R., Hutchinson, J.W., 1975. Bifurcation phenomena in the plane tension test. J. Mech. Phys. Solids 23, 239–264.

Hunt, G.W., Lord, G.J., Champneys, A.R., 1999. Homoclinic and heteroclinic orbits underlying the post-buckling of axially-compressed cylindrical shells. Comput. Meth. Appl. Mech. Engng. 170, 239–251.

Hutchinson, J.W., Miles, J.P., 1974. Bifurcation analysis of the onset of necking in an elastic/plastic cylinder under uniaxial tension. J. Mech. Phys. Solids 22, 61–71.

Hutchinson, J.W., Tvergaard, V., 1980. Surface instabilities on statically strained plastic solids. Int. J. Mech. Sci. 22, 339–354.

Karam, G.N., Gibson, L.J., 1995. Elastic buckling of cylindrical shells with elastic cores-I Analysis and II-Experiments. Int. J. Solids Struct. 32, 1259–1283 and 1285–1306.

Mehdizadeh, P., Block, R.J., 1972. The influence of anodic coatings on slip in aluminium. J. Electrochem. Soc.: Solid State Sci. Tech. 119, 1091–1094.

Miles, J.P., Nuwayhid, U.A., 1985. Bifurcation in compressible elastic/plastic cylinders under uniaxial tension. Appl. Sci. Res. 42, 33–54.

Needleman, A., 1979. Non-normality and bifurcation in plane strain tension or compression. J. Mech. Phys. Solids 27, 231–254.

Needleman, A., Ortiz, M., 1991. Effect of boundaries and interfaces on shear band localization. Int. J. Solids Struct. 28, 859–877.

Ogden, R.W., 1972. Large deformation isotropic elasticity – on the correlation of theory and experiment for incompressible rubberlike solids. Proc. R. Soc. Lond. A 326, 565–584.

Pan, F., Beatty, M.F., 1997a. Remarks on the instability of an incompressible and isotropic hyperelastic, thick-walled cylindrical tube. J. Elasticity 48, 217–239.

Pan, F., Beatty, M.F., 1997b. Instability of a Bell constrained cylindrical tube under end thrust – Part I: theoretical development. Math. Mech. Solids 2, 243–273.

Rittel, D., 1990. The influence of microstructure on the macroscopic patterns of surface instabilities in metals. Scripta Metall. Mater. 24, 1759–1764.

Rittel, D., Aharonov, R., Feigin, G., Roman, I., 1991. Experimental investigation of surface instabilities in cylindrical tensile metallic specimens. Acta Metall. Mater. 39, 719–724.

Rittel, D., Roman, I., 1989. Tensile deformation of coarse-grained cast austenitic manganese steels. Mater. Sci. Engng. A110, 77–87.

Seitzberger, M., Rammerstorfer, F.G., Degischer, H.P., Gradinger, R., 1997. Crushing of axially compressed steel tubes filled with aluminium foam. Acta Mechanica 125, 93–105.

Simpson, H.C., Spector, S.J., 1984. On barrelling instabilities in finite elasticity. J. Elasticity 14, 103–125.

Spencer, A.J.M., Rivlin, R., 1960. Further results on the theory of matrix polynomials. Arch. Rat. Mech. Anal. 4, 214–230.

Steif, P.S., 1986a. Bimaterial interface instabilities in plastic solids. Int. J. Solids Struct. 22, 195–207.

Steif, P.S., 1986b. Periodic necking instabilities in layered plastic solids. Int. J. Solids Struct. 22, 1571–1578.

Steif, P.S., 1987. An exact two-dimensional approach to fiber micro-buckling. Int. J. Solids Struct. 23, 1235–1246.

Steigmann, D.J., Ogden, R.W., 1997. Plane deformations of elastic solids with intrinsic boundary elasticity. Proc. R. Soc. Lond. A 453, 853–877.

Suo, Z., Ortiz, M., Needleman, A., 1992. Stability of solids with interfaces. J. Mech. Phys. Solids 40, 613–640.

Triantafyllidis, N., Maker, B.N., 1985. On the comparison between microscopic and macroscopic instability mechanisms in a class of fiber-reinforced composites. J. Appl. Mech. 52, 794–800.

Truesdell, C., Noll, W., 1965. The non-linear field theories of mechanics. In: Flügge, S. (Ed.), Encyclopedia of Physics vol. III/3, Springer, Berlin.

Vardoulakis, I., Sulem, J., 1995. Bifurcation Analysis in Geomechanics. Blackie, London.

Wilkes, E.W., 1955. On the stability of a circular tube under end thrust. Quart. J. Mech. Appl. Math. 8, 88–100.

Young, N.J.B., 1976. Bifurcation phenomena in the plane compression test. J. Mech. Phys. Solids 24, 77–91.

Zysset, P.K., Curnier, A., 1995. An alternative model for anisotropic elasticity based on fabric tensors. Mech. Mater. 21, 243–250.